Developmental, hormone- and stress-modulated expression profiles of four members of the Arabidopsis copper-amine oxidase gene family

Ilaria Fraudentali, Sandip A. Ghuge, Andrea Carucci, Paraskevi Tavladoraki, Riccardo Angelini, Renato A. Rodrigues-Pousada, Alessandra Cona

PII: S0981-9428(19)30502-9

DOI: https://doi.org/10.1016/j.plaphy.2019.11.037

Reference: PLAPHY 5952

To appear in: *Plant Physiology and Biochemistry*

Received Date: 11 October 2019

Revised Date: 22 November 2019

Accepted Date: 22 November 2019

Please cite this article as: I. Fraudentali, S.A. Ghuge, A. Carucci, P. Tavladoraki, R. Angelini, R.A. Rodrigues-Pousada, A. Cona, Developmental, hormone- and stress-modulated expression profiles of four members of the Arabidopsis copper-amine oxidase gene family, *Plant Physiology et Biochemistry* (2019), doi: https://doi.org/10.1016/j.plaphy.2019.11.037.

Contributions

AC and RA conceived the project. SG, RAR-P and AC designed the study. IF, SG, and ACa performed most of the experiments. All the authors contributed to data analysis. RAR-P and AC wrote the manuscript with contributions of RA, PT and the other authors.

Developmental, hormone- and stress-modulated expression profiles of four members of the Arabidopsis Copper-Amine Oxidase gene family

Ilaria Fraudentali[1*], Sandip A. Ghuge[2*], Andrea Carucci[1], Paraskevi Tavladoraki[1,3], Riccardo Angelini[1,3], Renato A. Rodrigues-Pousada[4] and Alessandra Cona[1,3]

[*]IF and SAG are joint first authors

Author affiliations

[1]**IF, ACa, PT, RA, and AC**, Department of Sciences, Università Roma Tre, Roma 00146, Italy;

[2]**SAG**, Institute of Plant Sciences, The Volcani Center, ARO, Bet Dagan 50250, Israel

[3]**PT, RA, and AC**, Istituto Nazionale Biostrutture e Biosistemi (INBB), Rome 00136, Italy;

[4]**RAR-P**, Department of Life, Health, and Environmental Sciences, Università dell'Aquila, L'Aquila 67100, Italy

Authors e-mail address

IF, ilaria.fraudentali@uniroma3.it; **SAG**, sandip.ghuge.biotech@gmail.com;

ACa, andrea.carucci@outlook.it; **PT**, paraskevi.tavladoraki@uniroma3.it;

RA, riccardo.angelini@uniroma3.it (orcid.org/0000-0002-1399-1187); **RAR-P**, pousada@univaq.it (orcid.org/0000-0003-2551-4705)

Corresponding author details

Alessandra Cona; e.mail: alessandra.cona@uniroma3.it; orcid.org/0000-0001-9039-8718

Department of Sciences, Università 'Roma Tre', Roma 00146, Italy; Istituto Nazionale Biostrutture e Biosistemi (INBB), Rome 00136, Italy;

Declarations of interest: none

Abstract

Copper-containing amine oxidases (CuAOs) catalyse polyamines (PAs) terminal oxidation producing ammonium, an aminoaldehyde and hydrogen peroxide (H_2O_2). Plant CuAOs are induced by stress-related hormones, methyl-jasmonate (MeJA), abscisic acid (ABA) and salicylic acid (SA). In the Arabidopsis genome, eight genes encoding CuAOs have been identified. Here, a comprehensive investigation of the expression pattern of four genes encoding AtCuAOs from the *α* and *γ* phylogenetic subfamilies, the two peroxisomal AtCuAOα2 (At1g31690) and AtCuAOα3 (At1g31710) and the two apoplastic AtCuAOγ1 (At1g62810) and AtCuAOγ2 (At3g43670), has been carried out by RT-qPCR and promoter::green fluorescent protein-β-glucuronidase fusion (GFP-GUS). Expression in hydathodes of new emerging leaves (*AtCuAOγ1* and *AtCuAOγ2*) and/or cotyledons (*AtCuAOα2*, *AtCuAOγ1* and *AtCuAOγ2*) as well as in vascular tissues of new emerging leaves and in cortical root cells at the division/elongation transition zone (*AtCuAOγ1*), columella cells (*AtCuAOγ2*) or hypocotyl and root (*AtCuAOα3*) was identified. Quantitative and tissue-specific gene expression analysis performed by RT-qPCR and GUS-staining in 5- and 7-day-old seedlings under stress conditions or after treatments with hormones or PAs, revealed that all four *AtCuAOs* were induced during dehydration recovery, wounding, treatment with indoleacetic acid (IAA) and putrescine (Put). *AtCuAOα2*, *AtCuAOα3*, *AtCuAOγ1* and *AtCuAOγ2* expression in vascular tissues and hydathodes involved in water supply and/or loss, along with a dehydration-recovery dependent gene expression, would suggest a role in water balance homeostasis. Moreover, occurrence in zones where an auxin maximum has been observed along with an IAA-induced alteration of expression profiles, support a role in tissue maturation and xylem differentiation events.

Keywords

Copper-amine oxidases, Polyamines, Auxin, Dehydration, Development, H_2O_2

Abbreviations[1]

1. Introduction

Polyamines (PAs) are nitrogen-containing compounds, present in all living organisms and essential for cell growth and differentiation. PAs play a multitude of functions in cells and although their biological roles remain somehow elusive, they interplay in basic cellular processes, including DNA replication and transcription, RNA modification, protein synthesis, regulation of ion-channel activities, free radical scavenging, cell cycle regulation as well as signal transduction pathways and programmed cell death. The fine regulation of their biosynthetic and catabolic pathways as well as conjugation and transport processes, which ensures an accurate homeostasis of PA cellular levels, also support the biological relevance of these compounds. Furthermore, besides their role in signal transduction pathways, PAs may act as sources of biologically active compounds such as hydrogen peroxide (H_2O_2) and aldehydes, generated via PA catabolism/interconversion pathways. In mammalian cells, dysregulation of PA metabolism has been linked to cancer development and owing to their role as modulators of cell proliferation and apoptosis, PAs have been target of antineoplastic therapies (Tavladoraki et al., 2012; Murray-Stewart et al., 2016).

In plants the PA spermidine (Spd), spermine (Spm) and their diamine precursor putrescine (Put), behave as modulators in signaling pathways involved in both developmental processes and responses to biotic and abiotic stresses (Jiménez-Bremont et al., 2014; Minocha et al., 2014; Tiburcio et al., 2014; Cai et al., 2015). Due to the elevated intracellular levels, PAs also represent

[1] **TPQ:** 2,4,5-trihydroxyphenylalanine quinone; **ABA:** Abscisic acid; **AOs:** Amine oxidases; **AtCuAOs:** Arabidopsis thaliana copper containing amine oxidases; **AtPAOs:** Arabidopsis thaliana polyamine oxidases; **BC:** Back conversion; **GUS:** β-glucuronidase; **CuAOs:** Copper containing amine oxidases; **FAD:** Flavin adenine dinucleotide; **PAOs:** Flavin adenine dinucleotide depending polyamine oxidases/Polyamine oxidases; **GFP:** Green fluorescence protein; **H_2O_2:** Hydrogen peroxyde; **IAA:** indoleacetic acid; **LSCM:** Laser scanning confocal microscopy; **MeJA:** Methyljasmonate; **NO:** Nitric oxide; **PAs:** Polyamines; **PI:** Propidium iodide; **PCD:** Programmed cell death; **Put:** Putrescine; **RT-qPCR:** Reverse transcription quantitative PCR; **ROS:** Reactive oxigene species; **SA:** Salicylic acid; **Spd:** Spermidine; **Spm:** Spermine; **TC:** Terminal catabolism; **T-Spm:** Thermospermine; **WT:** Wild type.

important sink of assimilated nitrogen (N) playing a role in the nitrogen/carbon balance by modulating biochemical pathways involved in carbon metabolism (Matoo et al., 2006). Furthermore, H_2O_2 derived from PA catabolism interplays in the complex network made up of reactive oxygen species (ROS) and nitric oxide (NO) produced by different plant enzymatic sources and alternatively driving harmful or signaling events, depending on its spatiotemporal signatures (Moschou et al., 2014; Gupta et al., 2016; Sobieszczuk-Nowicka et al., 2017).

PAs are oxidized through terminal or back-conversion metabolism giving rise to an amine moiety (that is ammonium, 1,3-diaminopropane or the corresponding lower level PA), an amino-aldehyde and H_2O_2 by two different classes of enzymes belonging to the amine oxidase (AO) family, that is FAD-containing polyamine oxidases (PAOs) and copper-containing amine oxidases (CuAOs), respectively oxidizing the carbon adjacent to the secondary or the primary amino group (Moschou et al., 2012; Tavladoraki et al., 2012; Tavladoraki et al., 2016). While PAOs include members that may catalyze either PA back-conversion metabolism (BC-PAOs) or terminal catabolism (TC-PAOs), CuAOs are exclusively responsible for terminal catabolism producing ammonium, an amino-aldehyde and H_2O_2 (Moschou et al., 2012; Tavladoraki et al., 2012; Tavladoraki et al., 2016). In most plant species, the preferred CuAO substrate is the diamine Put, these enzymes mostly showing a lower affinity for the higher PAs Spd and Spm, with some exceptions (Ghuge et al., 2015c; Tavladoraki et al., 2016). The ability to catalyze the terminal oxidation of Put and, in some cases, the first higher PA Spd, positions CuAOs at an early key step in the PA oxidative metabolism allowing them to behave as important regulators of PA levels in specific subcellular compartments.

In *Arabidopsis thaliana* five *PAO* genes (*AtPAOs*), that is the two encoding the cytosolic AtPAO1 and AtPAO5 and the three encoding peroxisomal AtPAO2-4 (Fincato et al., 2011; Ahou et al., 2014; Kim et al., 2014), and ten *CuAO* genes (*AtCuAOs*) are present, among which only eight encode for already characterized or still putative CuAOs, hereafter listed following nomenclature as previously proposed (Tavladoraki et al., 2016): *AtCuAOα1* (At1g31670); *AtCuAOα2* [At1g31690;

recently reported as *AtCuAO8* (Groß et al., 2017)]; *AtCuAOα3* [At1g31710; previously *AtCuAO2*, (Planas-Portell et al., 2013)]; *AtCuAOβ* [At4g14940; previously *ATAO1* or *AtAO1*, (Ghuge et al., 2015a)]; *AtCuAOγ1* [At1g62810; previously *AtCuAO1*, (Planas-Portell et al., 2013)]; *AtCuAOγ2* (At3g43670); *AtCuAOδ* [At4g12290, previously *AtCuAOδ2*, (Qu et al., 2014)]; *AtCuAOζ* [At2g42490; previously *AtCuAO3*, (Planas-Portell et al., 2013) or *AtCuAO1*, (Naconsie et al., 2014)]. The remaining two genes *AtCuAOε1* [*At4g12270*, previously *AtCuAOε*, (Qu et al., 2014)] and *AtCuAOε2* [*At4g12280;* previously *AtCuAOδ1* (Qu et al., 2014)] based on the alignment of their encoded proteins with the CuAO from *Pisum sativum*, have been shown to encode for proteins lacking essential active residues and supposed to be consecutive fragments of a copy of *AtCuAOδ* (Tavladoraki et al., 2016).

At present, some members belonging to the AtCuAO family have been only partially characterized at the biochemical and molecular level. Proteomic analysis studies revealed the presence of AtCuAOβ in the extracellular fluid (Boudart et al., 2005), AtCuAOδ in the vacuole (Carter et al., 2004) and AtCuAOα2 in the glyoxysomes (Fukao et al., 2003). Moreover, the analysis of the biochemical properties and subcellular localization of AtCuAO recombinant proteins showed that the apoplastic AtCuAOβ and AtCuAOγ1, the peroxisomal AtCuAOα3 and AtCuAOζ and the cytosolic/glyoxysomal AtCuAOα2 oxidize Spd at the primary amino group with an affinity comparable or slightly lower to that displayed for Put (Møller et al., 1998; Planas-Portell et al., 2013; Groß et al., 2017).

As it concerns the AO physiological roles, the cell-wall resident PAOs and CuAOs, detected at high levels in *Poaceae* and *Fabaceae* respectively, have been suggested to be involved in the H_2O_2 biosynthesis driving peroxidase-mediated cell wall cross-linking, as well as developmental and defense signaling pathways under biotic or abiotic stresses (Cona et al., 2006; Moschou et al., 2012; Ghuge et al., 2015b; Tavladoraki et al., 2016). Moreover, PAs may have a structural role in cell wall assembly and thickness (Berta et al., 1997). In this regard, owing to the absence in the apoplast of PA back-conversion metabolism along with the low levels/absence of detectable free

PAs, which are supposed to be secreted in the cell wall in response to environmental stresses, or at specific developmental stages, a role of apoplastic AOs in PA general homeostasis is reasonably unlikely (Yoda et al., 2003; Moschou et al., 2008; Ghuge et al., 2015c; Tavladoraki et al., 2016). Recently, growing attention has been focused on intracellular *Oryza sativa* and Arabidopsis BC-PAOs, which have been implicated in several cellular and physiological events, such as pollen tube growth, stomatal movement, fruit ripening, control of the thermospermine levels, xylem differentiation and salt/drought tolerance (Kim et al., 2014; Sagor et al., 2016; Tavladoraki et al., 2016; Alabdallah et al., 2017; Zarza et al., 2017). In this context, useful insights to progress in unravelling of *AtPAOs* physiological functions have been provided by the extensive characterization of their developmental expression patterns by promoter-GUS fusions (Fincato et al., 2012).

Less attention has been devoted to the physiological roles played by AtCuAOs. Planas-Portell et al. (Planas-Portell et al., 2013) reported a role for peroxisomal AtCuAOα3 and AtCuAOζ in PA homeostasis. AtCuAOγ1 has been firstly implicated in PA- and/or abscisic acid (ABA)-mediated NO production (Wimalasekera et at., 2011). Moreover, AtCuAOα2 has been shown to participate in NO production by influencing arginine availability through the modulation of arginase activity, suggesting a new regulatory pathway for NO production in plants (Groß et al., 2017). The AtCuAOβ-driven H_2O_2 production has been shown to signal the MeJA-mediated protoxylem differentiation in Arabidopsis roots, independently from the auxin/cytokinin/T-Spm loop (Ghuge et al., 2015a; Ghuge et al., 2015b) and promoter GFP-GUS evidence provided corroborating data. Considering that AtCuAOβ was also shown to be expressed in guard cells, a role in water balance homeostasis has been suggested for this protein (Ghuge et al., 2015b; Ghuge et al., 2015c). Furthermore, the guard cell resident AtCuAOζ has been hypothesized to be involved in the ABA-mediated control of stomata opening (Qu et al., 2014). This peroxisomal AtCuAO is up-regulated in response to ABA, MeJA, SA and flagellin suggesting a possible role in defense responses to biotic and abiotic stresses (Planas-Portell et al., 2013).

Herein, to lay the basis for future investigations on the roles played by different members of the AtCuAO family under physiological or pathological conditions, a comprehensive and extensive analysis of the early developmental-, stress-, hormone- and PA treatment-induced gene expression pattern of four *AtCuAOs* from the *α* and *γ* phylogenetic subfamilies, namely *AtCuAOα2*, *AtCuAOα3*, *AtCuAOγ1* and *AtCuAOγ2* (Tavladoraki et al., 2016), encoding for the two peroxisomal AtCuAOα2/α3 (α2, Fukao et al., 2003; α3, Planas-Portell et al., 2013) and the two apoplastic AtCuAOγ1/γ2 (γ1, Planas-Portell et al., 2013; γ2, http://suba.plantenergy.uwa.edu.au/flatfile.php?id=At3g43670), has been carried out. To this purpose, tissue-specific analysis of *AtCuAO*s expression patterns, exploiting promoter::*GFP-GUS* fusion transgenic plants, was integrated with quantitative investigation of gene expression by RT-qPCR analysis.

Our data reveal homogeneity and peculiarities in the tissue-specific expression pattern of these four *AtCuAOs*, suggesting shared physiological functions in plant developmental processes and abiotic stress responses in different tissues for each member.

2. Material and Methods

2.1. Plant materials, growth conditions and treatments

The Columbia (Col-0) ecotype of Arabidopsis was used as the wild-type (WT). Transgenic plants *prom-AtCuAO::GFP-GUS* of *AtCuAOα2* [*At1g31690*; TAIR (https://www.arabidopsis.org) accession number 2028636], *AtCuAOα3* (*At1g31710*; TAIR accession number 2028606), *AtCuAOγ1* (*At1g62810*; TAIR accession number 2026267) and *AtCuAOγ2* (*At3g43670*; TAIR accession number 2080173) were prepared by Gateway technology (Invitrogen) and plant transformation methods as described in the next paragraphs and/or sections.

Plants were grown in soil/perlite ratio 3:1 and/or *in vitro* in a growth chamber at a temperature of 23°C under long-day conditions (16/8 h photoperiod; 50 μmol m^{-2} s^{-1}). For *in vitro* growth, seeds were surface sterilized (Valvekens et al., 1988). After extensive washing with sterile water, seeds were stratified at 4°C for 2 days in the dark and then sown in ½ Murashige and Skoog

(MS) salt mixture (pH 5.7) supplemented with 0.5 (w/v) sucrose, 0.8% (w/v) agar (solid medium) and 50 $\mu g.mL^{-1}$ kanamycin (when antibiotic selection was necessary). Plates were placed vertically in the growth chamber.

Hormone and PA treatments as well as abiotic stress (wounding and dehydration) for RT-quantitative PCR (RT-qPCR) analysis of *AtCuAOα2, AtCuAOα3, AtCuAOγ1* and *AtCuAOγ2* genes were performed on 7-day-old WT seedlings grown for 6 days in solid medium and then transferred to ½ Murashige and Skoog (MS) salt mixture (pH 5.7) supplemented with 0.5 (w/v) sucrose (liquid medium) for one more day, as acclimation. After this period, for hormone/PA treatments liquid medium was replaced by fresh liquid medium containing the analyzed hormone or PA as follows: 100 μM ABA (Duchefa), 50 μM methyl jasmonate (MeJA; Duchefa), 2 mM salicylic acid (SA; Sigma-Aldrich), 10 μM 3-indolacetic acid (IAA), 500 μM putrescine (Put), 500 μM spermidine (Spd). Fresh liquid medium alone was used for control. For leaf-wounding analysis, cotyledons from acclimated seedlings were cut with scissors soon after liquid medium exchange, and then incubated in a growth chamber prior to be sampled at the time indicated below. For dehydration/recovery stress analysis, acclimated seedlings were left "drying" for 30 minutes (min) on an open plate under a ventilated hood. Material was collected before treatment (dehydration time 0) and immediately after this treatment (30 min dehydration). Fresh liquid medium was added to the plates and material was collected after the times indicated below for recovery time course (30 min dehydration represents 0 h recovery). Plant samples for gene expression studies were harvested at 0, 1, 3, 6 and 24 h frozen in liquid nitrogen and then kept at -80° C until RNA extraction.

To perform histochemical GUS and/or GFP analysis under light or confocal microscopy, seedlings were grown on solid medium supplemented with kanamycin and then used as hereafter described. In detail, 3-, 5-, 7-day-old *AtCuAOs-promoter::GFP-GUS* seedlings were used for analysis of early developmental tissue-specific gene expression. For the analysis of inducible tissue-specific gene expression upon hormone/PA treatments or abiotic stress, *AtCuAOs-promoter::GFP-GUS* 4-day-old (GUS and GFP analysis) or 6-day-old seedlings (GUS analysis) were transferred to

12-well tissue culture clusters containing liquid medium for 1 day. Then, the later was replaced with fresh liquid medium supplemented or not with the specific hormone/PA. For leaf-wounding and drought-stress GUS analysis, acclimated seedlings were treated as described for RT-qPCR analysis and sampled at relative mRNA-induction time. Samples were analyzed under Light- (LM) or Laser Scanning Confocal Microscopy (LSCM).

2.2. Cloning of the promoter region of four *AtCuAO*s and preparation of the corresponding *AtCuAO::GFP-GUS* transgenic plants

Transgenic plants expressing *prom-AtCuAO::GFP-GUS* constructs containing the promoter regions of *AtCuAOα2, AtCuAOα3, AtCuAOγ1* and *AtCuAOγ2* upstream of the GFP-GUS reporter construct were prepared as follows. Gateway technology was used to clone the regions upstream of the start codons of 2552 bp for *AtCuAOα2*, 2301 bp for *AtCuAOα3*, 2350 bp for *AtCuAOγ1* and 1788 bp for *AtCuAOγ2*. First, the *AtCuAO* promoter regions were amplified from Arabidopsis genomic DNA by PCR using sequence-specific primers (*promAtCuAO-for*/*rev*; Table 1) and cloned into the pDONR221 vector (Invitrogen) via Gateway technology (Invitrogen). The presence of the insert was confirmed by colony PCR carried out with the *promAtCuAO-for*/*rev* primers (Table 1) and by digestion of the purified plasmid with restriction enzymes (New England Biolabs) specific for either the vector or the sequence of the *AtCuAO* promoter region. The selected clones were further characterized to check for the presence of possible errors/mutations by sequencing with a pair of external primers (the standard *M13-for/rev* sequences) and internal primers (*prom-int-AtCuAO for/rev* in the case of *AtCuAOα2, α3 and γ1*, or just *prom-int-AtCuAO for* in the case of *AtCuAOγ2*; Table 2).

These promoter regions were successively inserted in a position upstream of the GFP-GUS fusion gene in the pKGWFS7 destination vector (Nakagawa et al., 2007). Constructs were introduced in *Agrobacterium tumefaciens* (strain GV301) and used to transform Arabidopsis WT by floral dip transformation (Clough & Bent, 1998). Selection of transgenic plants was performed

using solid medium supplemented with 50 µg.mL^{-1} kanamycin and PCR was carried out using primers specific for the *AtCuAO* promoters (*prom-int-AtCuAO for*) as well as primers specific for the enhanced green-fluorescent protein (*eGFP for/rev*) or the β-glucuronidase (*GUS for/rev*) genes (Table 2). Particularly, PCR reactions were carried out by using primer combinations such as *prom-int-AtCuAO-for*/*GFP-rev*, *GFP-for*/*GFP-rev* or *GUS-for*/*GUS-rev*. At least five transgenic lines per construct were analyzed at T1 generation by histochemical GUS staining at various developmental stages. Only highly reproducible results were taken into consideration for further analysis. Of the selected T1 generations, three independent transgenic lines, were subsequently followed (with confirmation of the kanamycin resistance and by PCR analysis), at the T2 and T3 generations with detailed examination of GUS and GFP activity.

Name of primer	Sequence of primer	Amplicon size
prom-*AtCuAOγ1-for*	5'-*GGGGACAAGTTTGTACAAAAAAGCAGGCT* CAACGACCAAGTCTCATCAATG-3'	**2350 bp**
prom-*AtCuAOγ1-rev*	5'-*GGGGACCACTTTGTACAAGAAAGCTGGGT* CGATTGAGTGAGAGTTTTTGAC-3'	
prom-*AtCuAOα3-for*	5'-*GGGGACAAGTTTGTACAAAAAAGCAGGCT* ATGAATGTGCAGAGATAGGGAAATA-3'	**2301 bp**
prom-*AtCuAOα3-rev*	5'-*GGGGACCACTTTGTACAAGAAAGCTGGGT* CTTTGTGAGGTATTATTGTTTGCTT-3'	
prom-*AtCuAOγ2-for*	5'-*GGGGACAAGTTTGTACAAAAAAGCAGGCT* CAAACAACAACAACTTGAACCTAGA-3'	**1788 bp**
prom-*AtCuAOγ2-rev*	5'-*GGGGACCACTTTGTACAAGAAAGCTGGGT* GGGAAGATCAGAAGATAAGTAACA-3'	
prom-*AtCuAOα2-for*	5'-*GGGGACAAGTTTGTACAAAAAAGCAGGCT* AGGGCTTAAAACATGAACGAGC -3'	**2552 bp**
prom-*AtCuAOα2-rev*	5'-*GGGGACCACTTTGTACAAGAAAGCTGGGT* TGCTTTGTGATTTGATTGAGTTGG-3'	

Table 1 Primers used for amplification of *AtCuAO* promoters and colony PCR. Sequences in italics correspond to the Gateway recombination recognition sites.

Name of primer	Sequence of primer
GFP-for	5′- GGTGAGCAAGGGCGAGGAGCTGTTC -3′

GFP-rev	5′- GTCGTCCTTGAAGAAGATGGTGCGCTC -3′
GUS-for	5′- CGTCCTGTAGAAACCCCAACCCGTGA -3′
GUS-rev	5′- CGGCGTGACATCGGCTTCAAATGGCG -3′
prom-int-AtCuAOγ1-for	5’- GAGGTTGGTTTCGAGTTTTCG - 3’
prom-int-AtCuAOγ1-rev	5’- AACGTGGAGATTTATGATGCTA -3’
prom-int-AtCuAOα3-for	5’- GGACCCGAGTGGTGATTGGA -3’
prom-int-AtCuAOα3-rev	5’- CCCTACCTACCTAACACATAATC -3’
prom-int-AtCuAOγ2-for	5’- GTGGTTAAGTCGTTGGTTCGGG -3’
prom-int-AtCuAOα2-for	5’- GGATGGTTATGGAAACTATATAGC- 3’
prom-int-AtCuAOα2-rev	5’- ATGTCTCGTCACCAAGAGGG- 3’

Table 2 Primers used for sequencing of the amplified *AtCuAO* promoters and control of the transgenic lines.

2.3. Genomic DNA and RNA extraction, PCR and RT-qPCR analysis

Genomic DNA was isolated from young leaf tissue of 15-day-old Arabidopsis seedlings as previously described (Fulton et al., 1995) and 100 ng were used to amplify DNA fragments.

For promoter region cloning, the PCR reactions were carried out with the Platinum® Pfx DNA polymerase (Invitrogen) in an *iCycler* ^{TM} *Thermal Cycler* (Bio-Rad) following the manufacturer’s instructions with the following parameters: 95°C for 2 min then 30 cycles of 95°C for 20 s, 55-60°C for 20 s, 72°C for 15-60 s/kb, followed by a final extension at 72°C for 3 min.

For screening PCR (bacterial colonies and transgenic seedlings), the PCR reaction was carried out with the BIOTAQ DNA Polymerase (Bioline) with the following parameters: 95°C for 2 min then 35 cycles of 95°C for 30 s; 55-60°C for 60 s; 72°C for 60 s.kb^{-1}, followed by a final extension at 72°C for 10 min.

Total RNA was isolated from Arabidopsis seedlings (100 mg) by using TRIzol® Reagent (Invitrogen) following the manufacture’s instruction with slightly modifications. To eliminate traces of genomic DNA, RNA samples were treated with RNase-Free DNase Set (QIAGEN).

Quantitative expression profiles of *AtCuAOα2, AtCuAOα3, AtCuAOγ1* and *AtCuAOγ2* genes were determined by RT-quantitative PCR (RT-qPCR) on 7-day-old whole Arabidopsis seedlings after different treatments. In detail, RT-qPCR analysis was performed on DNase-treated RNA (4

µg) as follows. cDNA synthesis and PCR amplification were carried out using *GoTaq® 2-Step RT-qPCR System200* (Promega) following manufacturer's protocol. The first cDNA strand was synthesized using random and oligo *dT* primers in an *iCycler* ^{TM} *Thermal Cycler* (Bio-Rad) with the following parameters: 25°C for 5 min, 42°C for 60 min and 70°C for 15 min. The PCRs were run in a Corbett RG6000 (Corbett Life Science, QIAGEN) utilizing the following program: 95°C for 2 min then 40 cycles of 95°C for 7 s and 60°C for 40 s. The melting program ramps from 60°C to 95°C rising by 1°C each step. *AtCuAOα2, AtCuAOα3, AtCuAOγ1* and *AtCuAOγ2* specific primers were *qPCR-AtCuAO for-rev* (Table 3). Ubiquitin-conjugating enzyme 21 (UBC21, At5g25760) was used as reference gene and specific primers were prepared [*UBC21-for* and *UBC21-rev*; Table 3 (Czechowski et al., 2005)]. The software used to control the thermocycler and to analyze data was the Corbett Rotor-Gene 6000 Application Software (version 1.7, Build 87; Corbett Life Science, QIAGEN). Fold change in the expression of the *AtCuAO* genes were calculated according to the $\Delta\Delta C_q$ method as previously described (Livak & Schmittgen., 2001; Fraudentali et al., 2019).

Name of primer	Sequence of primer
UBC21-for	5′- CTGCGACTCAGGGAATCTTCTAA -3′
UBC21-rev	5′- TTGTGCCATTGAATTGAACCC -3′
AtCuAOα2-qPCR-for1	5′- GACGACACATTAGCCGTATGGTC -3′
AtCuAOα2-qPCR-rev1	5′- AAGCCGCCAAACATAGTAGGCA -3′
AtCuAOα3- qPCR-for1	5′- ATTACGGAGGTTAGACCGGACG -3′
AtCuAOα3- qPCR-rev1	5′- CCGTGTATGTCTTCCCCTAGTT -3′
AtCuAOγ1- qPCR-for1	5′- GCTGGCGACATTCTGAGATCC -3′
AtCuAOγ1- qPCR-rev1	5′- CACCATTAACATTCCCGAAGCC -3′
AtCuAOγ2- qPCR-for1	5′- CACAAACAATCAGATATGGGTGA -3′
AtCuAOγ2- qPCR-rev1	5′- CACTATGTCCTTGTTCTCAATGG -3′

Table 3. Primers used for RT-qPCR analysis on 7-day-old whole Arabidopsis seedlings after different treatments.

2.4. Histochemical analysis of GFP signal and GUS assay

Investigation of constitutive and inducible tissue-specific expressions was carried out by histochemical GUS and GFP analysis under light or confocal microscopy, respectively. GFP and

propidium iodide (PI; 10 µg.mL^{-1}, Sigma-Aldrich) fluorescence, with the later used to reveal cell outlines, were analyzed using a Leica TCS-SP5 confocal microscope equipped with an Argon laser emitting at the wavelength of 488 nm. Analyzes were performed exploiting the Leica Application Suite Advanced Fluorescence-LAS-AF software selected emission band ranging from 505 to 560 nm for GFP analysis and from 600 to 680 nm for PI staining.

GUS staining was performed as previously described (Jefferson, 1987). Samples were gently soaked in 90% (v/v) cold acetone for 30 min at -20°C for prefixation and rinsed 3 times with 50 mM sodium phosphate buffer pH 7.0. After that, plant material was immersed in the staining solution (1 mM 5-bromo-4-chloro-3-indolyl-β-D-glucuronide, 2.5 mM potassium ferrocyanide, 2.5 mM potassium ferricyanide, 0.1% (v/v) Triton X-100, 10 mM EDTA, 50 mM sodium phosphate buffer, pH 7.0) under *vacuum*. For early developmental tissue-specific gene expression, the reaction proceeded overnight at 37°C in dark. Histochemical GUS staining following hormone/abiotic stress treatments was allowed to proceed until differences in the intensity between treated and untreated plants were detected under the microscope. Chlorophyll was extracted by several washings; first with ethanol/acetic acid ratio 1:3 (v/v) for 30 min, then with ethanol/acetic acid ratio 1:1 (v/v) for 30 min and finally with 70% ethanol. Samples were stored in 70% ethanol at 4°C, prior to being observed under light microscopy. For early developmental and inducible tissue-specific gene expression, images were acquired by a Leica DFC450C digital camera applied to a Zeiss Axioplan2 microscope. Shown images of whole plants were reconstructed aligning overlapping micrographs of the same seedling.

For cross-sections analyzes, 5-day-old GUS-stained seedlings were embedded in Technovit 7100 resin (Heraeus Kulzer) following the manufacture's instruction and 20 µm sections were obtained using a Microm HM330 microtome. Images were acquired under the light microscope Zeiss Axioplan 2, equipped with a Leica DFC450C digital camera.

2.5. GUS and GFP experimental set-up and RT-qPCR statistics

The analysis by GUS staining and GFP fluorescence of the early developmental tissue-specific gene expression in seedlings at different ages (3-, 5- and 7-day-old), was carried out on a minimum of thirty plants from three independent transgenic lines. Five sections of each plant organ were observed.

The analysis by GUS staining and GFP fluorescence of the hormone-, PA- and abiotic stress-inducible tissue-specific gene expression was performed on a minimum of ten seedlings per treatment from five independent experiments, utilizing the most representative transgenic line. Images from single representative experiments are shown.

For RT-qPCR analysis of at least three biological replicates each with three technical replicates were performed. Statistical tests were performed using GraphPad Prism (GraphPad Software) with One-way ANOVA analysis followed by Sidak's multiple comparison tests. Statistical significance of differences was evaluated by *P* level. *ns*, not significant *P* value > 0.05; *, **, *** and **** *P* values ≤ 0.05, 0.01, 0.001 and 0.0001 respectively.

3. Results

3.1. Expression pattern analysis of the AtCuAOs α and γ phylogenetic branches

Phylogenetic analysis based on amino acid sequence identity (Additional file 1: Fig. S1) revealed that members of the AtCuAO (Copper amine oxidases, E.C. 1.4.3.6) family are clustered in three different clades, so being represented in each of the three plant CuAO family clades (Tavladoraki et al., 2016): in particular clade I include AtCuAOβ, AtCuAOα1, AtCuAOα2 and AtCuAOα3, clade II AtCuAOδ, AtCuAOε1, AtCuAOε2, AtCuAOγ1 and AtCuAOγ2 and clade III AtCuAOζ. The alignment of the aminoacid sequences of the AtCuAO putative proteins encoded by the ten genes annotated as *AtCuAOs* with that of *Pisum sativum* CuAO (referred as PSAO), revealed that eight of them include all the active site residues crucial for the catalytic activity, except for AtCuAOε1 and AtCuAOε2 (Additional file 2: Fig. S2). In detail, PSAO possess five active site residues essential for catalysis namely His442, His444 and His603 involved in copper coordination,

Tyr387 precursor of the topaquinone (TPQ) cofactor and Asp300 (Kumar et al., 1996), while AtCuAOε2 and AtCuAOε1 respectively lack Asp300 and His442/444/603/Tyr387 residues (PSAO numbering; Additional file 2: Fig. S2). It has been hypothesized that *AtCuAOε1* and *AtCuAOε2*, located upstream of *AtCuAOδ* on chromosome 4, could be fragments arisen from a copy of the latter generated by a duplication event (Tavladoraki et al., 2016), that was successively followed by the insertion of the transposable element *At4g12275* (The Arabidopsis Information Resource; https://www.arabidopsis.org).

Considering that except for AtCuAOζ which is in clade III, most of the AtCuAOs are clustered in clade I and II, we have chosen to focus on members belonging to the latter major branches of the phylogenetic tree. Concerning clade I, as several studies are already available about AtCuAOβ tissue-specific expression and physiological roles (Ghuge et al., 2015a, Ghuge et al., 2015b, Ghuge et al., 2015c), the attention has been focused on the α members, especially AtCuAOα2 and AtCuAOα3 that present a peculiar developmental pattern of expression of the corresponding genes based on EFP browser (http://bar.utoronto.ca/efp/cgi-bin/efpWeb.cgi) data. Furthermore, considering that the δ/ε sub-branch in clade II includes only one-member encoding for a putative functional enzyme, AtCuAOδ, which has been object of a recent study (Fraudentali et al., 2019), we have decided to follow through with the analysis of the two members of the γ sub-branch.

Here the developmentally-regulated and tissue-specific expression patterns of *AtCuAOα2*, *AtCuAOα3*, *AtCuAOγ1* and *AtCuAOγ*2 genes have been investigated by analysis of promoter::*GFP-GUS* fusion transgenic plants at 3, 5 and 7 days after germination. Moreover, the hormone-induced tissue-specific expression patterns of these four *AtCuAOs* have been explored by treatments with four different hormones, among which the growth regulator IAA and the three stress-related hormones ABA, MeJA and SA (Verma et al., 2016), selected on the basis of data retrieved from the Arabidopsis EFP Browser [http://bar.utoronto.ca/efp/cgi-bin/efpWeb.cgi; (Winter et al., 2007)] and/or available in literature (Cona et al., 2006; Wimalasekera et at., 2011; Moschou et al., 2012; Planas-Portell et al., 2013; Ghuge et al., 2015a; Ghuge et al., 2015c; Tavladoraki et al., 2016; Groß

et al., 2017). To integrate the stress-related hormone analysis, the effect of two different abiotic stresses, dehydration/recovery and wounding, were also investigated. Furthermore, we analyzed the effects of two PAs, Put and Spd, on the expression of the four *AtCuAO* genes. The qualitative data obtained were supported by a quantitative analysis of the *AtCuAO* expression profiles by RT-qPCR analysis.

3.2. Analysis of tissue-specific expression pattern of *AtCuAOα2* during early development

Figure 1 shows that at all the analyzed developmental stages, promoter-driven GUS expression and GFP signal were exclusively observed in leaves. In 3-day-old seedlings, a diffuse spotted GUS staining was detectable in cotyledonary leaves (Fig. 1a and b) characterized by a more intense staining in hydathodes (Fig. 1c) and leaf borders (Fig. 1b and c). Moreover, a clearly detectable promoter activity was revealed also in leaf primordia (Fig. 1d). Likewise, in 5-day-old seedlings, a widespread promoter activity with intense GUS staining in cotyledonary leaf borders and hydathodes was observed as well (Fig. 1e- g) along with a strong promoter-driven GUS expression in expanding first leaves (Fig. 1f and h). Analysis of promoter-driven GFP signal in 5-day-old seedlings, showed fluorescence in epidermal cells of cotyledons (Fig. 1i and j) and young leaf margins (Fig. 1k). Conversely, in cotyledonary leaves of 7-day-old seedlings, promoter activity was restricted to the external margins (Fig. 1l), even remaining at high levels in cotyledonary hydathodes (Fig. 1m) and in new emerging leaves (Fig. 1n).

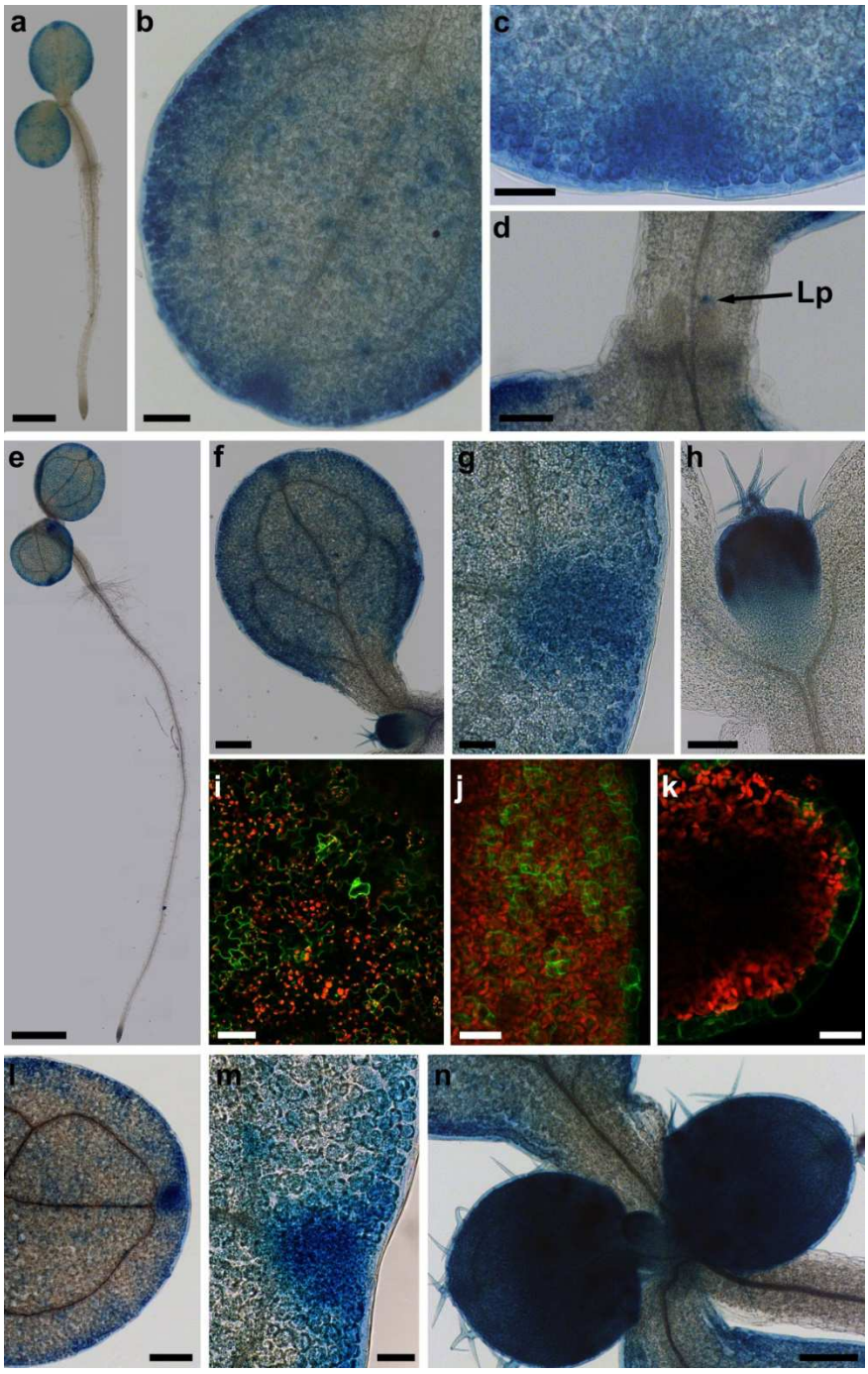

Figure 1. *AtCuAOα2* tissue expression pattern in 3- 5- and 7-day-old *AtCuAOα2-promoter::GFP-GUS* Arabidopsis transgenic seedlings by light microscopy analysis after GUS staining and LSCM analysis of GFP signal.

3.3. Analysis of tissue-specific expression pattern of *AtCuAOα3* during early development

Figure 2 shows that *AtCuAOα*3 expression is mainly detectable in stipules, hypocotyl and root. Indeed, analysing GUS-stained 3-day-old seedlings (Fig. 2a), it was possible to detect promoter activity in shoot apex where staining was associated with stipules (Fig. 2b) as well as in hypocotyl (Fig. 2b, c), hypocotyl/root junction (Fig. 2d) and root mature zone (Fig. 2e), where

*AtCuAOα*3 expression was especially detected in vascular tissue. This expression pattern remained stable in 5-day-old seedlings (Fig. 2f) where promoter activity was detected in stipules (Fig. 2g), hypocotyl (Fig. 2h), hypocotyl/root junction (Fig. 2i), and root mature zone (Fig. 2j). Analyzing longitudinal sections from 5-day-old seedlings, it was possible to observe the presence of GUS staining in shoot apex where staining was associated with stipules (Fig. 2k), and in hypocotyl, especially in xylem vessels (Fig. 2l). Cross sections of hypocotyl (Fig. 2m), hypocotyl/root junction (Fig. 2n) and root mature zone (Fig. 2o) confirmed what observed with longitudinal sections, showing promoter activity in metaxylem vessels. Seven-day-old seedlings maintained the same expression patterns compared to those shown by 3- and 5-day-old plants (Fig. 2p-s).

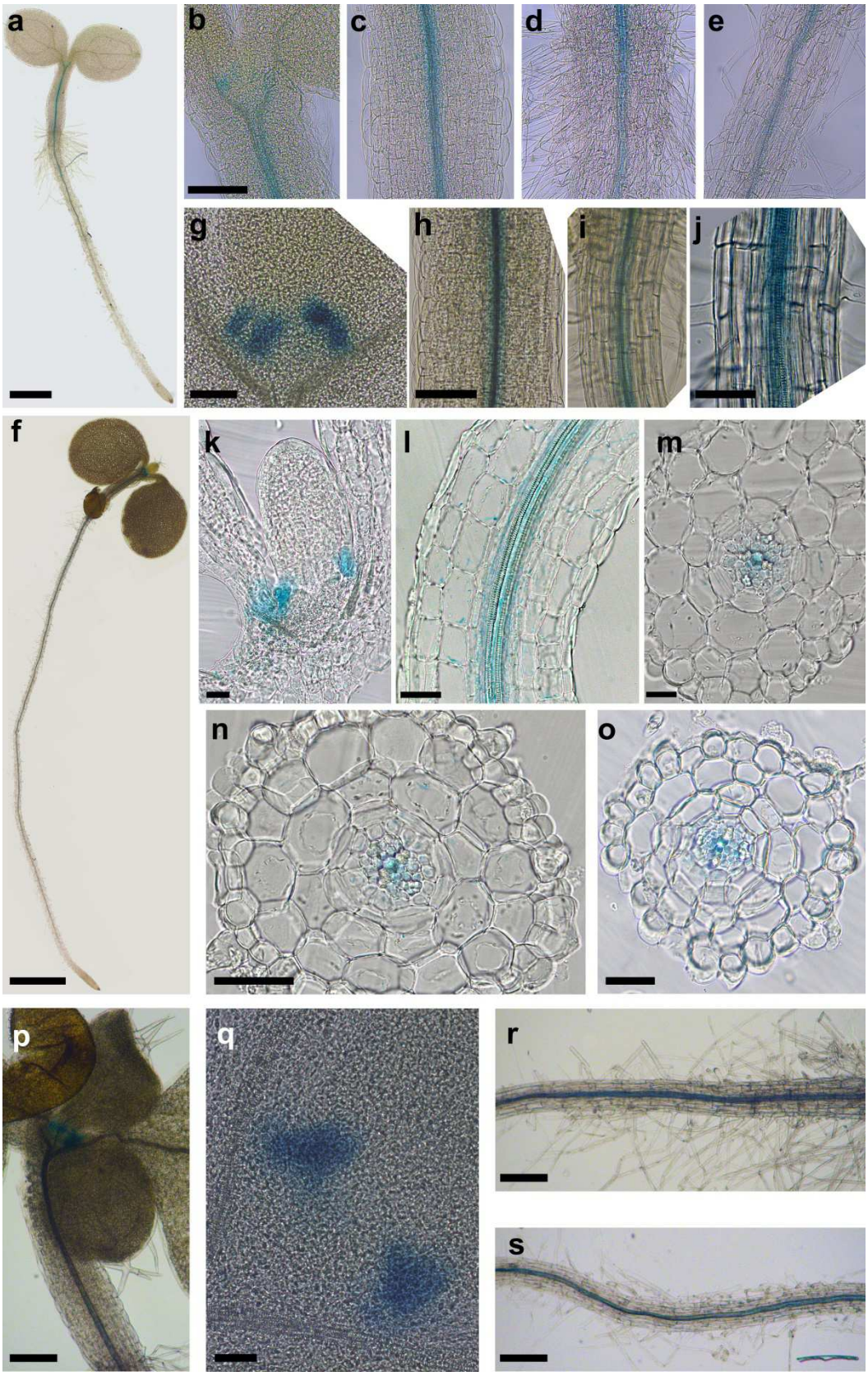

Figure 2. *AtCuAOα3* tissue expression pattern in 3-, 5- and 7-day-old *AtCuAOα3-promoter::GFP-GUS* transgenic seedlings and sections by light microscopy analysis after GUS staining.

3.4. Analysis of tissue-specific expression pattern of *AtCuAOγ1* during early development

In 3-day-old *AtCuAOγ1-promoter::GFP-GUS* seedlings (Fig. 3a-g), GUS staining revealed an intense promoter activity in shoot apex (Fig. 3b), in hypocotyl and hypocotyl/root junction (Fig. 3d), and in root apex particularly at the transition and elongation zone (Fig. 3g). Staining was also detected in the apical tip of cotyledons (Fig. 3c) and in root mature zone (Fig. 3e). Five-day-old transgenic plants (Fig. 3h-l) showed strong promoter activity in root apex, especially at the transition and elongation zones (Fig. 3l). A weaker promoter activity was revealed in the apical meristem (Fig. 3j) as well as in vascular tissues of cotyledons (Fig. 3i) and developing leaf primordia (Fig. 3k). Analyzing GFP fluorescence in sequential root sections from the epidermis to the central zone of primary root apex from 5-day-old *AtCuAOγ1-promoter::GFP-GUS* plants under confocal microscopy, it was possible to detect in more detail promoter activity in cortical cell files, at the transition and elongation zones (Fig. 3m and n). In root mature zone, GFP signal was also associated with epidermal cells (Fig. 3o). Analysis of 7-day-old plants showed a strong promoter activity in hydathodes and vascular tissues of cotyledons (Fig. 3p) and young leaf (Fig. 3q and r) that were respectively weaker and stronger than those observed in cotyledons and leaf primordia of 5-day-old plants. Moreover, a fainter GUS staining was observed in the root mature zone (Fig. 3s and t).

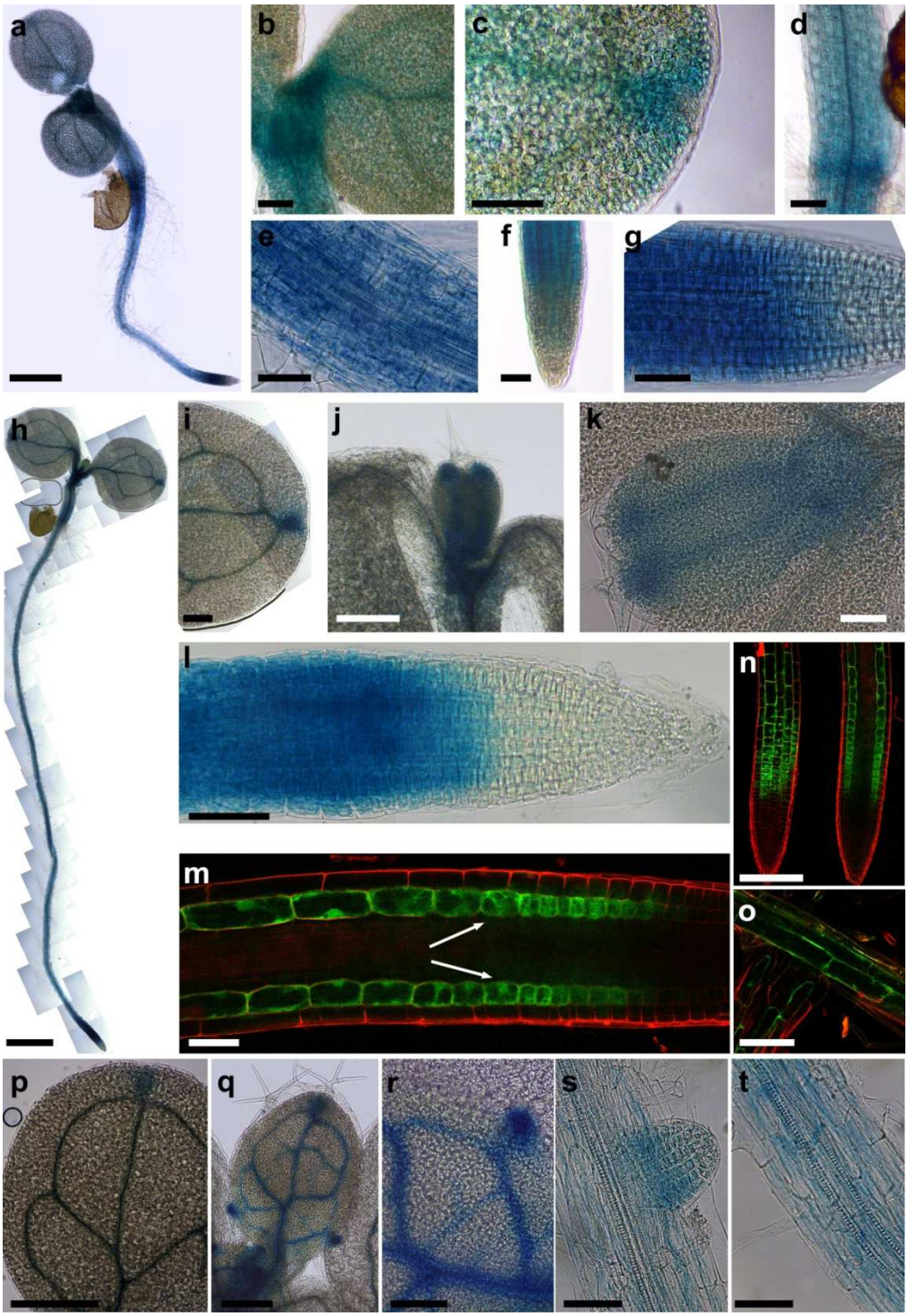

Figure 3. *AtCuAOγ1* tissue expression pattern in 3-, 5- and 7-day-old *AtCuAOγ1-promoter::GFP-GUS* transgenic seedlings by light microscopy analysis after GUS staining and LSCM analysis of GFP signal.

The analysis of cross- and tangential-sections of cotyledons from 5-day-old *AtCuAOγ1-promoter::GFP-GUS* plants showed promoter activity in the vascular tissues (Fig. 4a-e). Furthermore, observation of longitudinal sections revealed promoter-driven GUS staining in the

shoot apex, in particular at the junction between leaf primordia and hypocotyl (Fig. 4f-h), in roots (Fig. 4i-k) as well as in hypocotyl and hypocotyl/root junction always associated with vascular tissue (Fig. 4l-o). In details, the analysis of root longitudinal sections confirmed the occurrence of promoter activity in cortical cell files of mature and transition/elongation zones (Fig. 4i and j) coherently to what observed with GFP analysis (Fig. 3m and n). Moreover, cross-sections analysis showed that GUS staining was strongly associated with vascular tissue in hypocotyl (Fig. 4l) and cortical cell files in roots (Fig. 4k and p). A weaker expression was observed in epidermis of hypocotyl (Fig. 4k) and root (Fig. 4p).

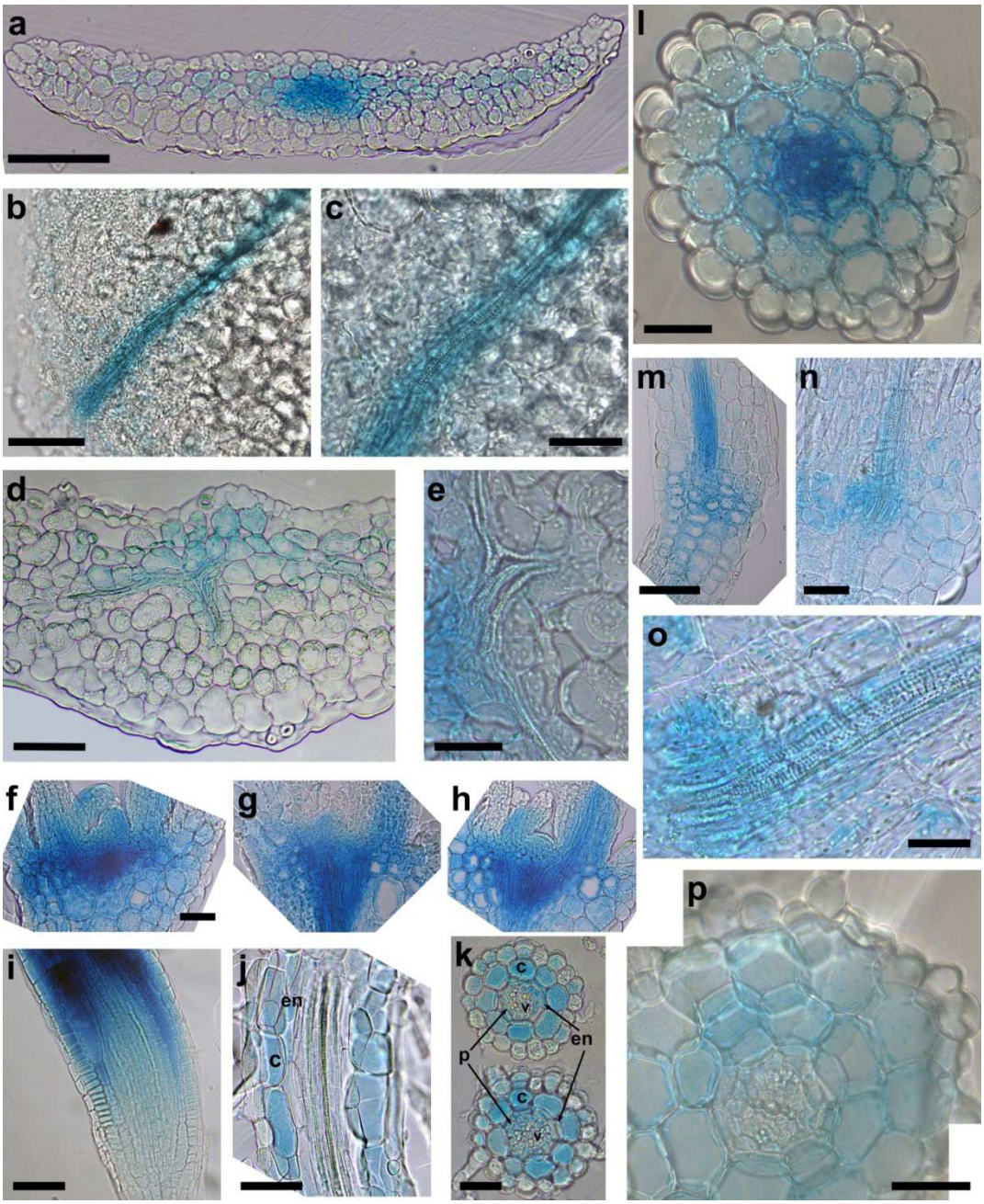

Figure 4. *AtCuAOγ1* tissue expression pattern in sections of 5-day-old *AtCuAOγ1-promoter::GFP-GUS* transgenic Arabidopsis seedlings by light microscopy analysis after GUS staining.

3.5. Analysis of tissue-specific expression pattern of *AtCuAOγ2* during early development

Analysis of 3-day-old *AtCuAOγ2-promoter::GFP-GUS* plants (Fig. 5a) revealed strong promoter activity in hydathodes of cotyledons (Fig. 5b), in hypocotyl/root junction (Fig. 5d), hypocotyl (Fig. 5c) and in root apex (Fig. 5e). At the following developmental stages, namely at the age of 5-days, promoter activity staining was very intense in root apex (Fig. 5l). GUS staining was also clearly visible in root mature zone, especially at the root/hypocotyl junction (Fig. 5k).

Moreover, like what was observed in 3-day-old plants, GUS staining was evident in hydathodes of cotyledons (Fig. 5g) and appeared also in apical hydathodes of newly formed expanding leaves (Fig. 5i and j). GFP analysis of 5-day-old seedlings strongly supported data so far described. Indeed, the GFP fluorescence was visible in the hydathode zone of cotyledons (Fig. 5h). Moreover, GFP signal was detectable in columella cells (Fig. 5m and n). Seven-day-old *AtCuAOγ2-promoter::GFP-GUS* plants showed a pattern of promoter activity similar to what was observed in 5-day-plants (Fig. 5o-r).

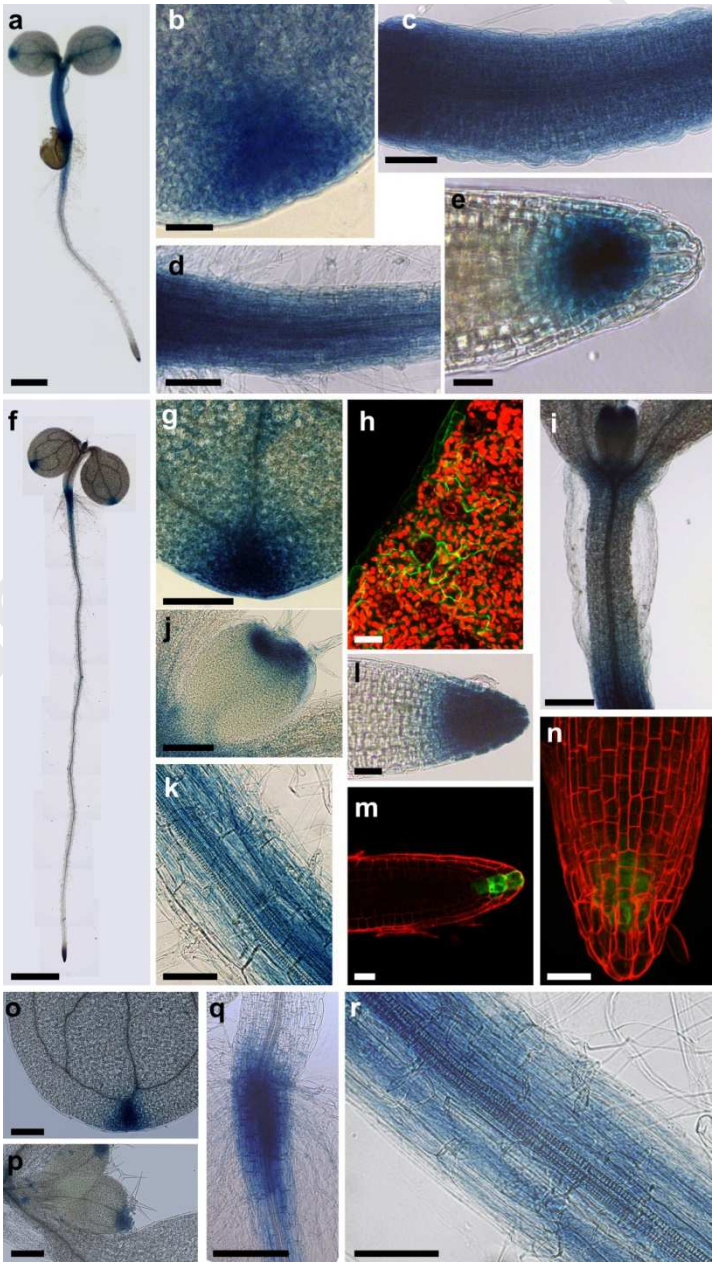

Figure 5. *AtCuAOγ2* tissue expression pattern in 3-, 5- and 7-day-old *AtCuAOγ2-promoter::GFP-GUS* Arabidopsis transgenic seedlings by light microscopy analysis after GUS staining and LSCM analysis of GFP signal.

Analysis of longitudinal- and cross-sections of 5-day-old seedlings, allowed us to further confirm what was observed in whole plants. Indeed, longitudinal- and cross-sections of root tip (Fig. 6a and b) confirmed the occurrence of a strong promoter activity in whole root cap. Cross-sections of root mature zone revealed a prevalent promoter activity in epidermis and in cortical cells while a lower expression was observed in endodermis cells (Fig. 6c and d). The analysis of hypocotyl longitudinal- and cross-sections showed the occurrence of promoter-driven GUS staining in epidermis and cortical cells (Fig. 6e and f), similar to root mature zone. Moreover, the analysis of tangential- and cross-sections of cotyledons (Fig. 6g-l) showed a strong staining around the central vascular bundle in the hydathode zone (Fig. 6g, h, k, l), while longitudinal sections of shoot apex exhibited a clear staining in the apical zone of leaf primordia (Fig. 6i and j).

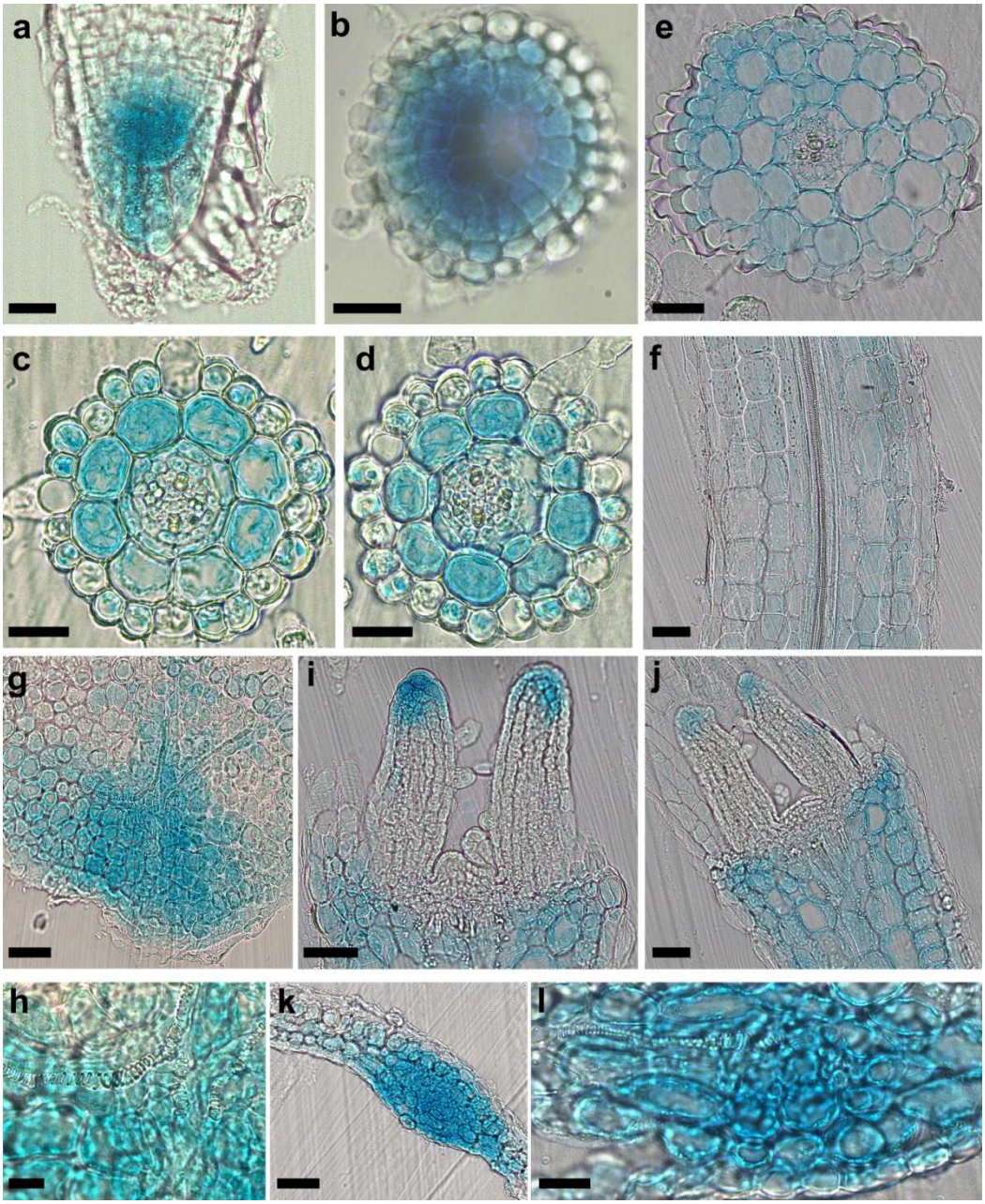

Figure 6. *AtCuAOγ2* tissue expression pattern in sections of 5-day-old *AtCuAOγ2-promoter::GFP-GUS* transgenic seedlings by light microscopy analysis after GUS staining.

3.6. Expression profile of *AtCuAOα2* and *AtCuAOα3* after treatment with auxin and the stress-related hormones, MeJA, ABA and SA

Similar modulation of the expression profiles of *AtCuAOα2* and *AtCuAOα3* by auxin (IAA), MeJA, ABA and SA were highlighted by RT-qPCR analysis. IAA (10 µM) induced an initial peak followed by a repression, MeJA induced expression of both genes while ABA and SA showed a down-regulating effect (Fig. 7). In particular, IAA induced the expression of *AtCuAOα2* of 3.6- and

3.2-fold at 1 and 3 h respectively. The strong repression effect, 20% of control untreated plants (T0), was visible only at the 24 h time-point (Fig. 7a). The effect of IAA induction on *AtCuAOα3* expression was significant albeit at a lower level (2- and 1.4-fold at the same time points) than for *AtCuAOα2*. The observed repression effect was visible earlier, but at a lower level than for *AtCuAOα2*, being 40% of T0 at 6 and 24 h time-point (Fig. 7b). On the other hand, 50 µM MeJA induced *AtCuAOα2* expression by 2.7- and 2.4- fold respectively after 6 and 24 h from the treatment onset, while no significant changes were observed after 1 and 3 h in comparison with T0 (Fig. 7c). Similarly, a strong induction of *AtCuAOα3* expression was observed after the same treatment. In detail, we observed an initial 4-fold induction after 3 h, followed by a 5-fold and 4-fold-induction after 6 and 24 h respectively, from the treatment onset in comparison with T0 (Fig. 7d). Upon 100 µM ABA treatment, *AtCuAOα2* and *AtCuAOα3* expression rapidly decreased during the period of the time course analysis. In particular, we observed 40%, 67% and 90% decrease of *AtCuAOα2* gene expression after 3, 6 and 24 h from the treatment onset in respect to T0, while after 1 h no significant differences were visible (Fig. 7e). Furthermore, a similar profile of *AtCuAOα3* gene expression was observed with 80% and 90% decrease after 6 and 24 h from the treatment onset with no significant differences after 1 and 3 h in respect to T0 (Fig. 7f). A decrease in *AtCuAOα2* and *AtCuAOα3* expression was also observed upon 2 mM SA treatment. Specifically, no significant differences in *AtCuAOα2* expression profile were observed after 1 and 3 h from the treatment onset as compared with that observed in T0, while *AtCuAOα2* expression levels decreased by 50% and 80% at 6 and 24 h respectively (Fig. 7g). Moreover, *AtCuAOα3* expression level showed no significant differences up to 6 h from the treatment onset, while at 24 h a 72% decrease was observed compared with T0 (Fig. 7h).

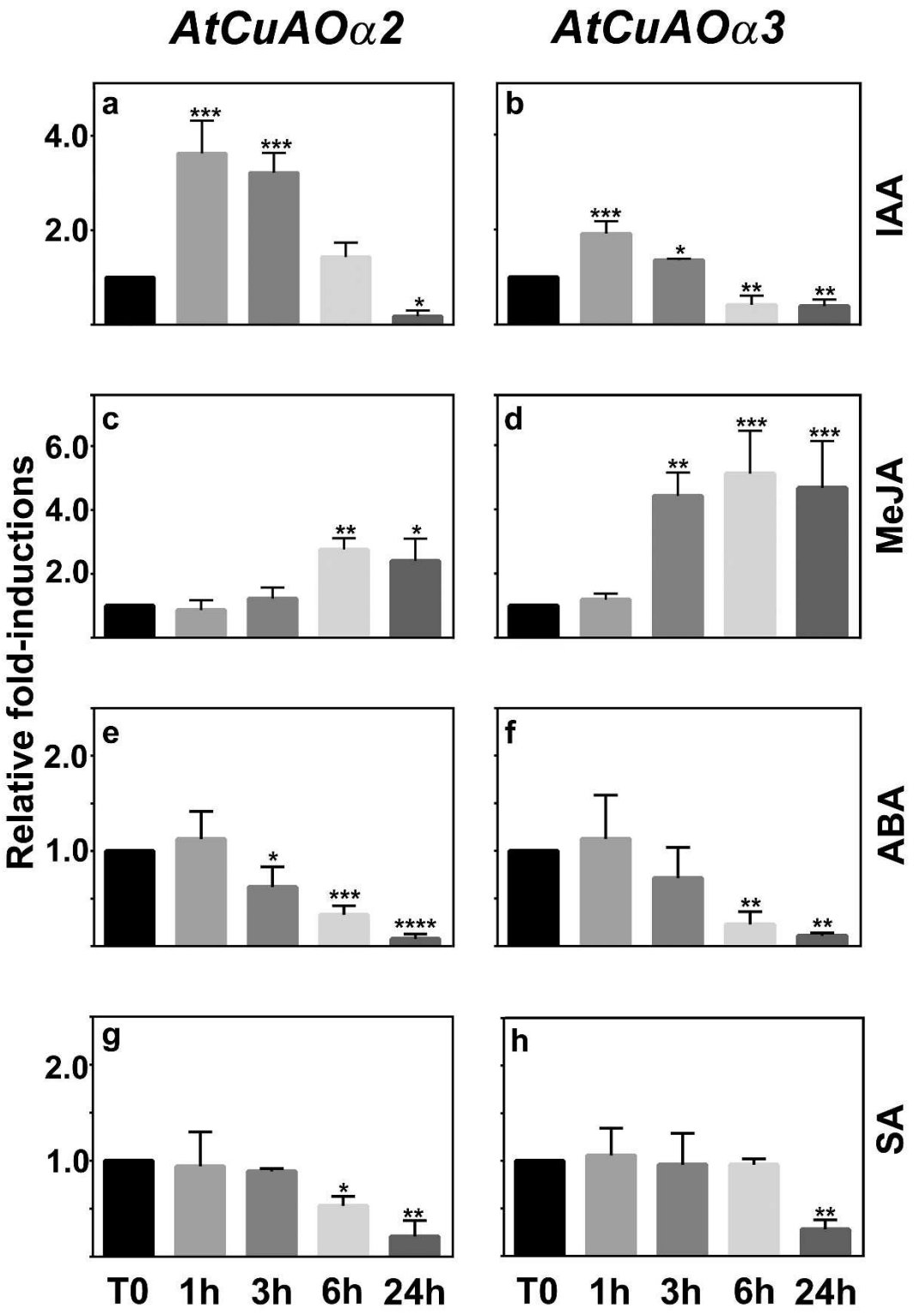

Figure 7. Time-course analysis of *AtCuAOα2* and *AtCuAOα3* gene expression by RT-qPCR upon treatment with IAA, MeJA, ABA and SA.

Considering data from RT-qPCR, the analysis of the tissue specific expression pattern of *AtCuAOα2* and *AtCuAOα3* after IAA and MeJA treatments have been carried out using *promoter::GFP-GUS* plants. IAA induced *AtCuAOα2* expression in cotyledons and newly formed

expanding leaves, especially in hydathodes and epidermis (Fig. 8a-d), as revealed by the presence of an intense GUS staining at the external border of cotyledons (Fig. 8b) as well as at the hydathodes of new emerging leaves (Fig. 8d), as compared to control untreated plants (Fig. 8a and c). Furthermore, IAA induced *AtCuAOα3* expression (Fig. 8k-n) in stipules, in the petiole/apex junction (Fig. 8l) and remarkably in the stele of root mature zone (Fig. 8n), as compared to control untreated plants (Fig. 8k and m). MeJA induced *AtCuAOα2* expression in cotyledons and newly formed expanding leaves, especially in hydathodes and epidermis (Fig. 8e-j), as revealed by the presence of a more intense GUS staining at the apical hydathode (Fig. 8f) and at the external border of cotyledons (Fig. 8h) as well as at the hydathodes of new emerging leaves (Fig. 8j), as compared to control untreated plants (Fig. 8e, g, i). Furthermore, MeJA induced *AtCuAOα3* expression (Fig. 8o-t) in stipules (Fig. 8p), in the hypocotyl stele and in hypocotyl/root junction (Fig. 8r), and principally in the stele of root mature zone (Fig. 8r). Particularly, analysis of GFP signal (Fig. 8s-t) revealed that in root mature zone of MeJA treated plants, gene expression was induced in the vascular tissue (Fig. 8t) as compared to untreated plants, in which fluorescence was barely detectable (Fig. 8s).

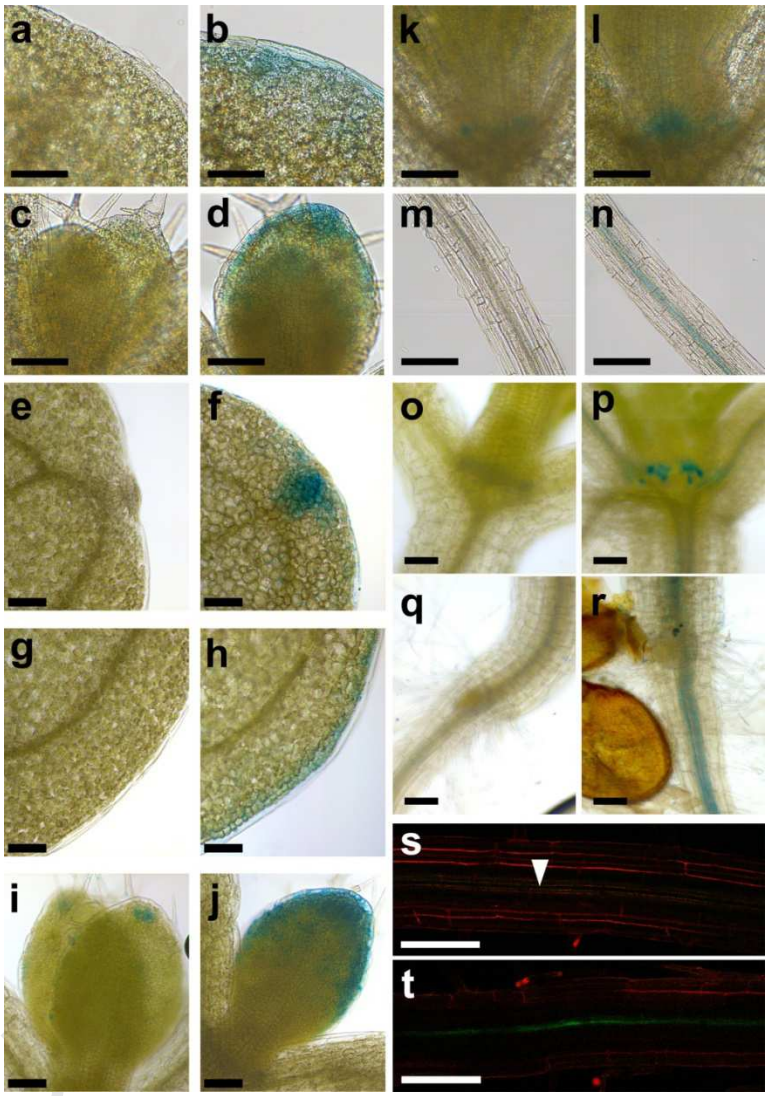

Figure 8. Analysis of *AtCuAOα2* and *AtCuAOα3* tissue specific expression pattern upon IAA and MeJA treatments.

3.7. Expression profile of *AtCuAOα2* and *AtCuAOα3* after dehydration/recovery and wounding stress

To correlate the *AtCuAOα2* and *AtCuAOα3* gene expression profiles after ABA and MeJA treatments with the responses of the same genes to the main ABA and MeJA-signaled abiotic stresses, the variations of *AtCuAOα2* and *AtCuAOα3* gene expression profiles under dehydration and successive recovery, and upon leaf wounding (Fig. 9) were analyzed.

As shown in Fig. 9, after 30 min dehydration (T1) no apparent changes in the expression levels (Fig. 9, inset in both upper panels) were highlighted for both genes while significant changes

were observed during the successive Dehydration Recovery (DR). In particular, *AtCuAOα2* presented peaks of expression at T3 and T4 (3 and 6 h DR) with 4-fold inductions that returned to T0 levels at T5 (24 h DR), while *AtCuAOα3* presented a peak from T2 to T3 (2-fold induction at 1 and 3 h DR) that were no longer significantly different from T0 levels at T4 and T5 (Fig. 9, upper right and left panels). Upon leaf-wounding, *AtCuAOα2* expression presented a small but significant peak (1.6-fold) of induction at 1 h time point, followed by a quick return to T0 levels (Fig. 9, lower left panel), while *AtCuAOα3* expression presented an induction from 1 to 6 h time points with a strong induction peak at 3 h (2-fold for 1 and 6 h, 4-fold at 3 h) returning to T0 levels at 24 h (Fig. 9, lower right panel).

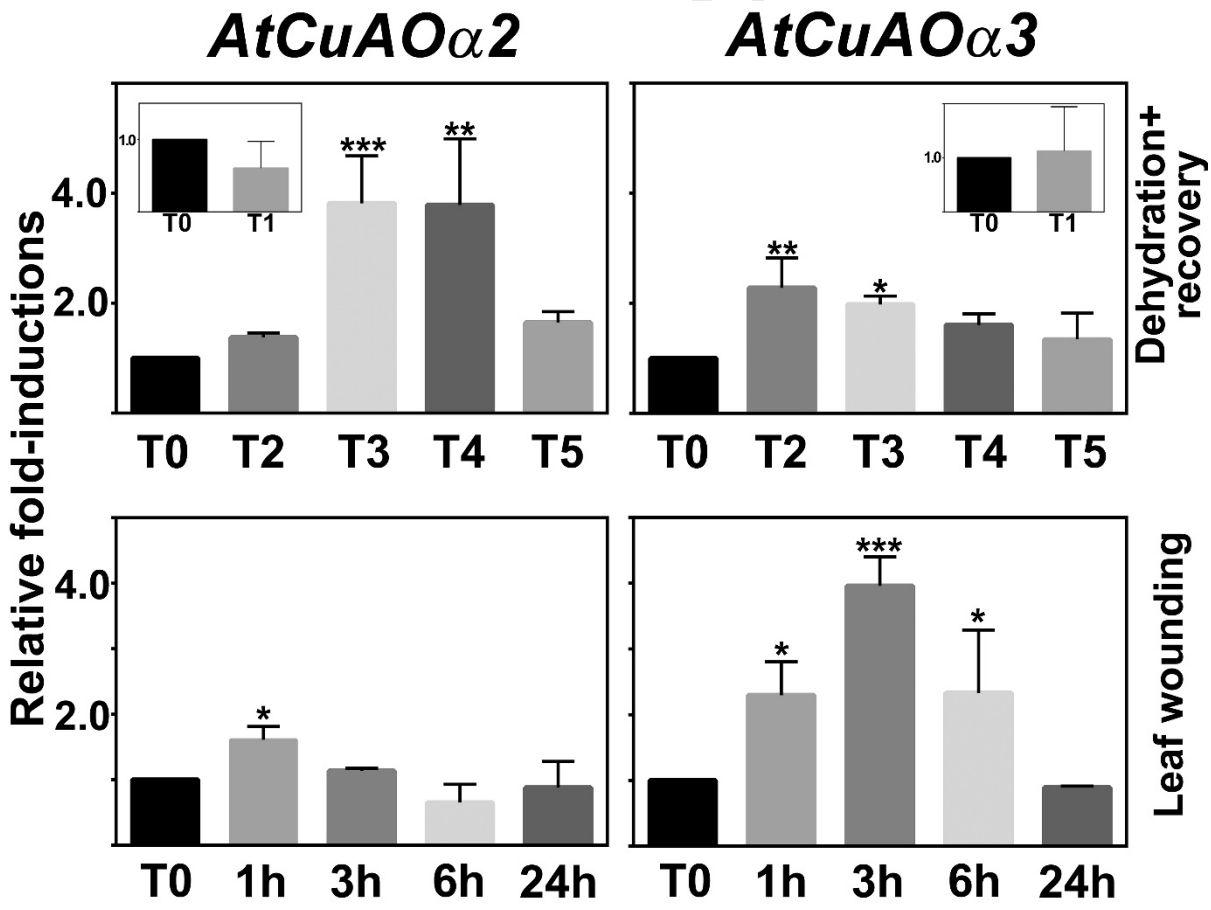

Figure 9. Time-course analysis of *AtCuAOα2* and *AtCuAOα3* gene expression by RT-qPCR upon abiotic stress treatments (dehydration and recovery and leaf wounding).

Considering data from RT-qPCR, the analysis of the tissue-specific expression pattern of *AtCuAOα2* and *AtCuAOα3* after these stress treatments have been carried out. Both DR and leaf

wounding stresses induced *AtCuAOα2* expression in cotyledon margins and newly formed expanding leaves, especially in hydathodes and epidermis (Fig. 10a-f), as revealed by the presence of an intense GUS staining at the external border of cotyledons (Fig. 10d and f) as well as in the hydathodes and in leaf margins of new emerging leaves (Fig. 10c and e) of stressed *AtCuAOα2-promoter::GFP-GUS* plants as compared to control untreated plants (Fig. 10a and b). Furthermore, both stresses induced *AtCuAOα3* expression (Fig. 10g-l) in stipules (Fig. 10i and k), and in the stele of root mature zone (Fig. 10j and l) as compared to control untreated plants (Fig. 10g and h).

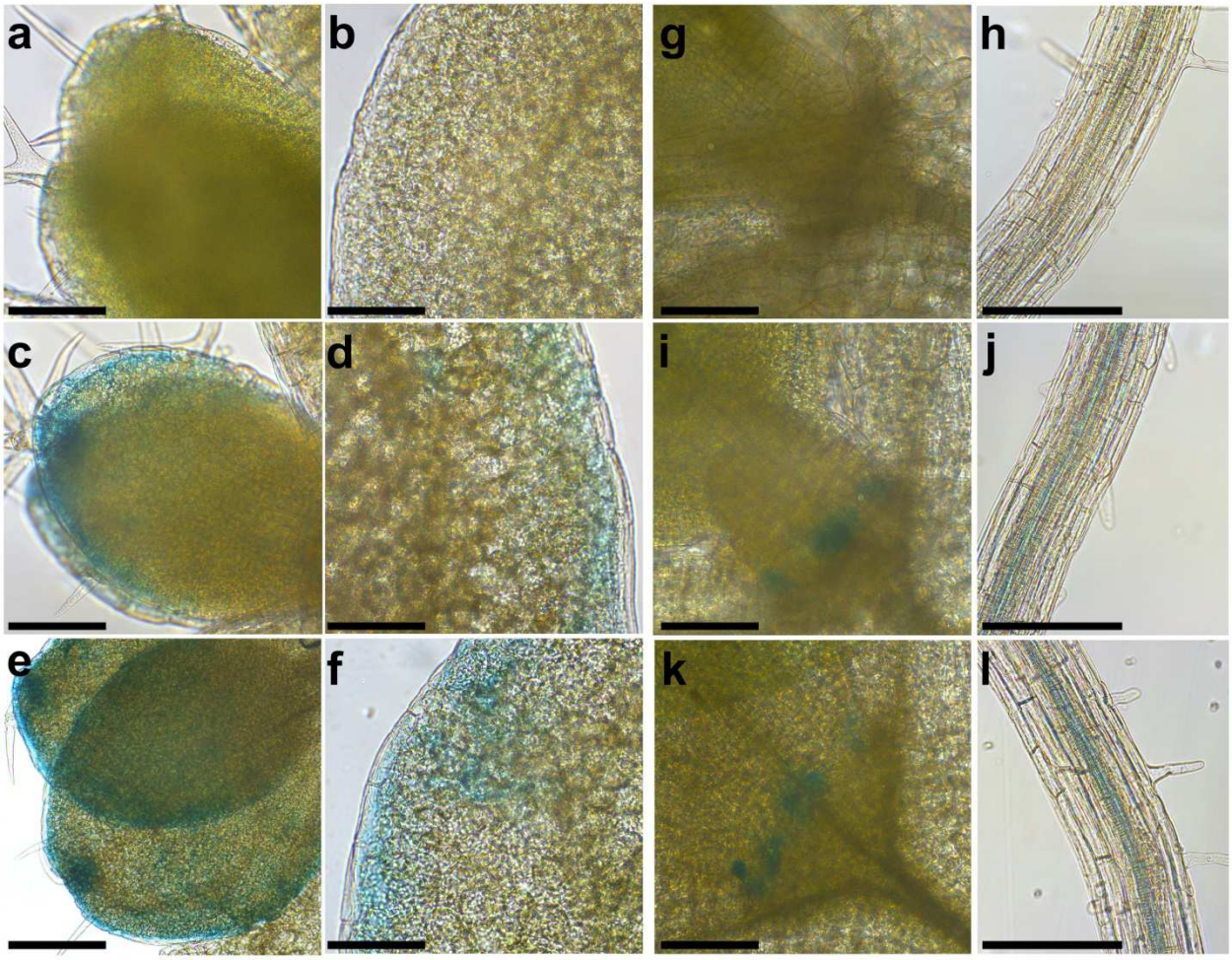

Figure 10. Analysis of *AtCuAOα2* and *AtCuAOα3* tissue-specific expression pattern upon abiotic stress (leaf wounding and dehydration recovery) treatments.

3.8. Expression profile of *AtCuAOα2* and *AtCuAOα3* after treatment with PAs

To verify the occurrence of a direct effect of exogenous Put and Spd on the expression profile of the clade I genes presented in this study, RT-qPCR analysis has been carried out on plants treated with Put or Spd at the final concentration of 500 µM.

As shown in Fig. 11, treatments with Put and Spd had different effects on the expression of these clade I genes (Fig. 11). Treatment with 500 µM Put induced *AtCuAOα2* at the late 24 h time point (2-fold) while it was maintained at T0 levels at 1, 3 and 6 h (Fig. 11, upper left panel). Instead, Put strongly induced *AtCuAOα3* from 1 h time point (2-fold) up to 6 h (3-fold), only returning to T0 levels at the latest time point studied (Fig. 11, upper right panel). Responses to 500 µM Spd treatment presented opposite time course profiles for *AtCuAOα2* and for *AtCuAOα3* with induction peaks of 4- and 2-fold at 3- and 24 h for the former (Fig. 11 Lower left panel), and a strong repression at 6 h (20%) which returned approximately to T0 levels at 24 h (1.4-fold) for the latter (Fig. 11, lower right panel).

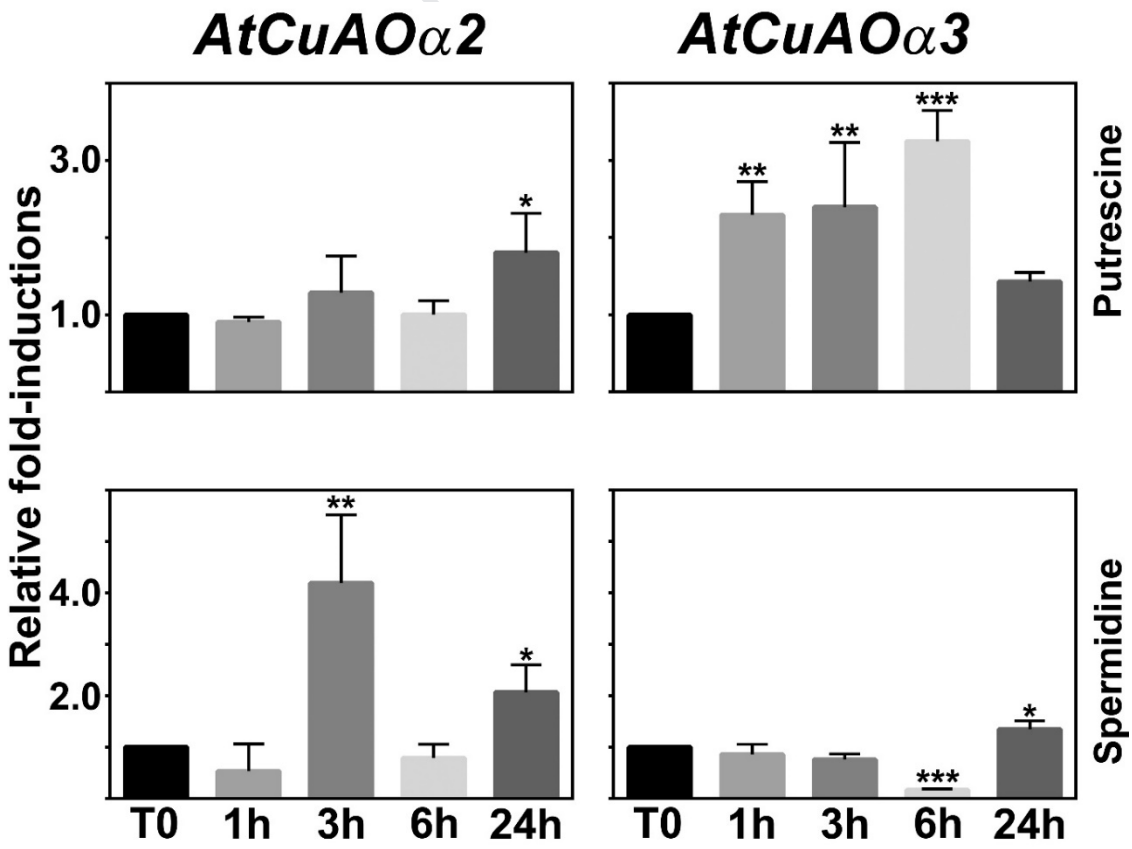

Figure 11. Time-course analysis of *AtCuAOα2* and *AtCuAOα3* gene expression by RT-qPCR upon treatment with the polyamines putrescine e spermidine.

Considering data from RT-qPCR, the analysis of the tissue specific expression pattern of *AtCuAOα2* and *AtCuAOα3* after Put and Spd treatments have been carried out. Both PAs induced *AtCuAOα2* expression in cotyledon margins and newly formed expanding leaves, especially in hydathodes and epidermis (Fig. 12a-f), as revealed by the presence of an intense GUS staining in the hydathodes and in leaf margins of new emerging leaves (Fig. 12c and e) as well as in the hydathodes of cotyledons (Fig. 12d and f) of Put- and Spd-treated *AtCuAOα2-promoter::GFP-GUS* plants as compared to control untreated plants (Fig. 12a and b). Furthermore, Put induced *AtCuAOα3* expression (Fig. 12g-j) in the stele of root mature zone (Fig. 12h) and in stipules (Fig. 12j), as compared to control untreated plants (Fig. 12g and i).

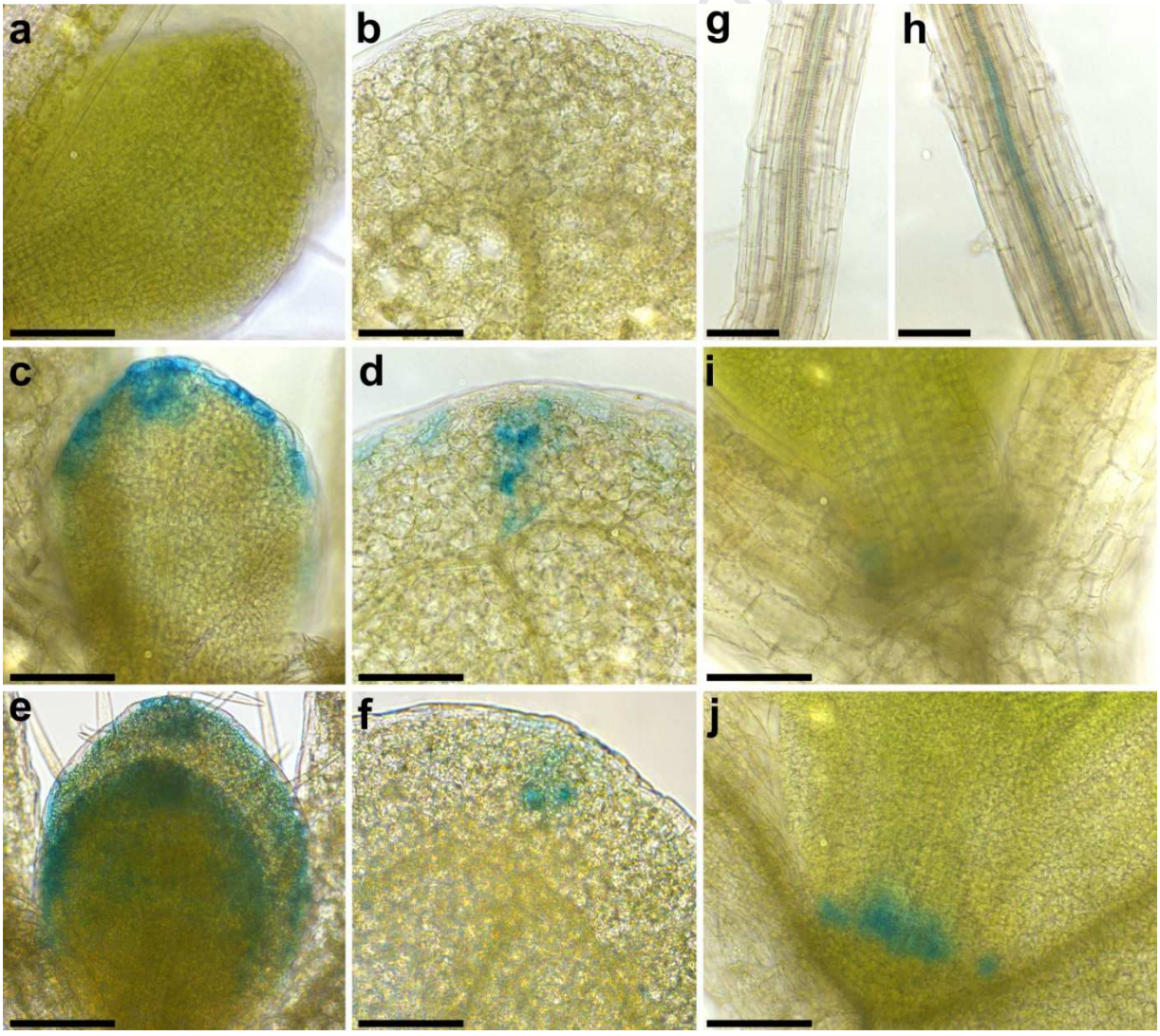

Figure 12. Analysis of *AtCuAOα2* and *AtCuAOα3* tissue specific expression pattern upon putrescine or spermidine treatment.

3.9. Expression profile of *AtCuAOγ1* and *AtCuAOγ2* after treatment with auxin and the stress-related hormones, MeJA, ABA and SA

The quantitative analysis of *AtCuAOγ1* and *AtCuAOγ2* expression by RT-qPCR upon treatment with IAA showed similar profiles between these clade II genes with an initial induction (2-fold) followed by return to T0 levels or a repression (40%) at the late time point (24 h). Concerning the action of the three stress-related hormones analyzed on the expression profiles of these two genes, induction effects were observed on *AtCuAOγ1* expression upon ABA and SA treatments, while repressive or no effect was observed for all the other treatments (Fig. 13). In particular, IAA (10 µM) induced *AtCuAOγ1* expression of approximately 2-fold from 1 to 6 h. This effect was no longer visible at the 24 h time point (Fig. 13a). A significant 2-fold induction of *AtCuAOγ2* expression was observed at the 3 h time point, while a repression effect was clear at the last time point studied (40%) when compared to T0 (Fig. 13b). After treatment with 50 µM MeJA, no significant changes in *AtCuAOγ1* expression profile occurred at each analyzed time point as compared with T0 (Fig. 13c), while a 40% and 50% decrease of *AtCuAOγ2* expression was revealed respectively at 1 and 3 h (Fig. 13d). Treatment with 100 µM ABA induced *AtCuAOγ1* expression by 2-fold after 3 h from the treatment onset (Fig. 13e) while a 60 % decrease of *AtCuAOγ2* expression was detected after 24 h (Fig. 13f). On the other hand, 2 mM SA-treated plants showed a 50% decrease of *AtCuAOγ1* (Fig. 13g) and *AtCuAOγ2* (Fig. 13h) expression respectively upon 1 h of treatment in respect to T0 and a 1.8-fold increase of *AtCuAOγ1* expression after 6 h of treatment.

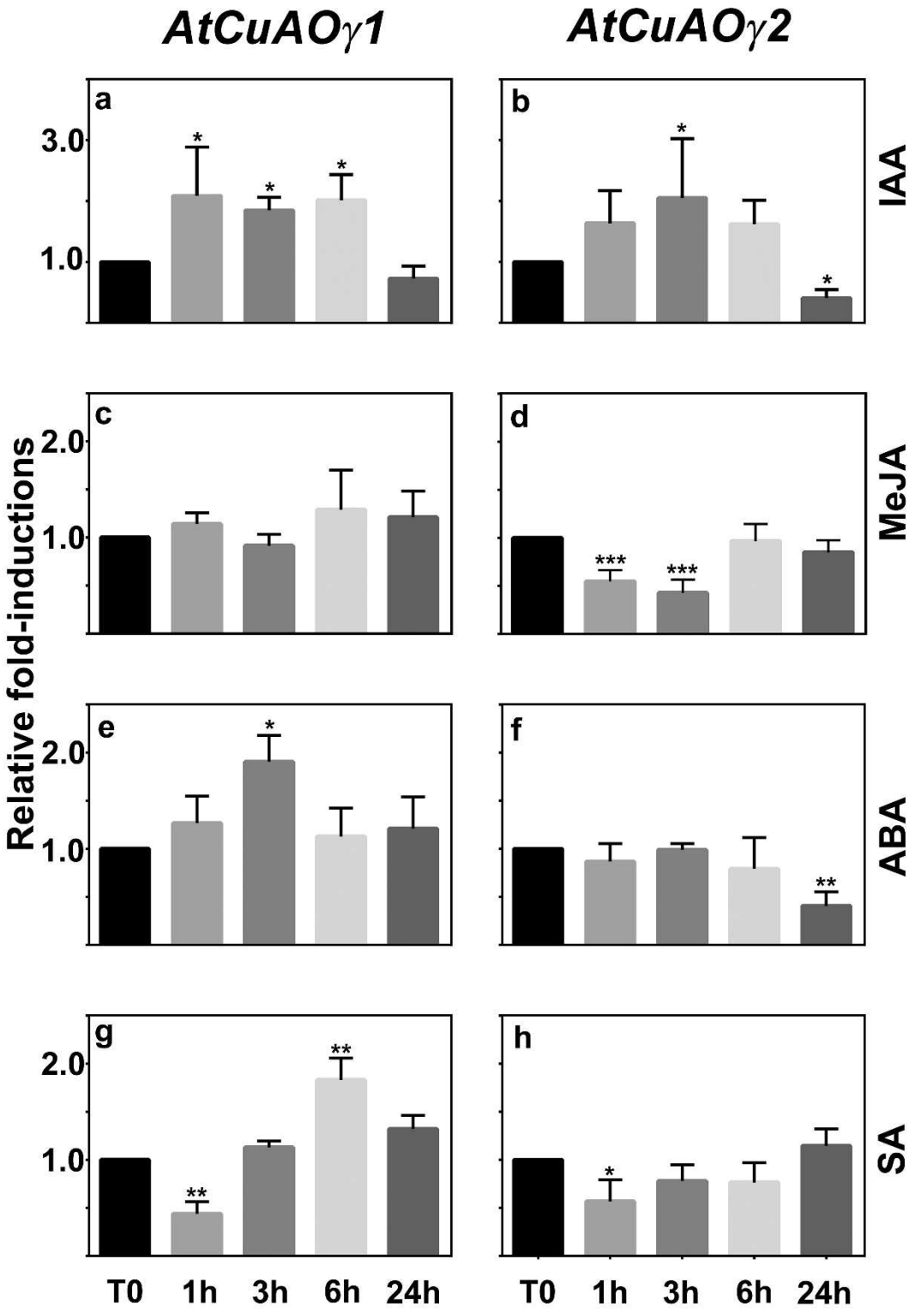

Figure 13. Time-course analysis of *AtCuAOγ1* and *AtCuAOγ2* gene expression by RT-qPCR upon treatment with IAA, MeJA, ABA and SA.

Considering data from RT-qPCR, a GUS staining analysis was carried out to investigate the IAA-induced tissue specific expression pattern for both *AtCuAOγ1* and *AtCuAOγ2* while the ABA- and SA-induced tissue specific expression pattern was explored only for *AtCuAOγ1* (Fig. 14).

Consistently, IAA-treated *AtCuAOγ1-promoter::GFP-GUS* plants displayed a stronger blue staining in the root elongation zone (Fig. 14a) as compared to control untreated plants (Fig. 14b). ABA-treated *AtCuAOγ1-promoter::GFP-GUS* plants displayed a more intense promoter driven GUS-staining in root transition/elongation zone as compared with control untreated plants (Fig. 14c and d). Moreover, while SA induced *AtCuAOγ1* expression in the same root zone (Fig. 14e and f) the tissue specific expression pattern revealed that the promoter activity detectable in the ground tissues of the root elongation zone in control untreated plants (Fig. 14e) spread towards the ground tissues of the root maturation zone upon SA treatment (Fig. 14f). IAA induced *AtCuAOγ2* expression in the columella (Fig 14h) and the stipules of young emerging leaves (Fig. 14j) as revealed by the presence of a more intense GUS staining in IAA-treated *AtCuAOγ2-promoter::GFP-GUS* plants when compared with control untreated plants (Fig. 14g and i).

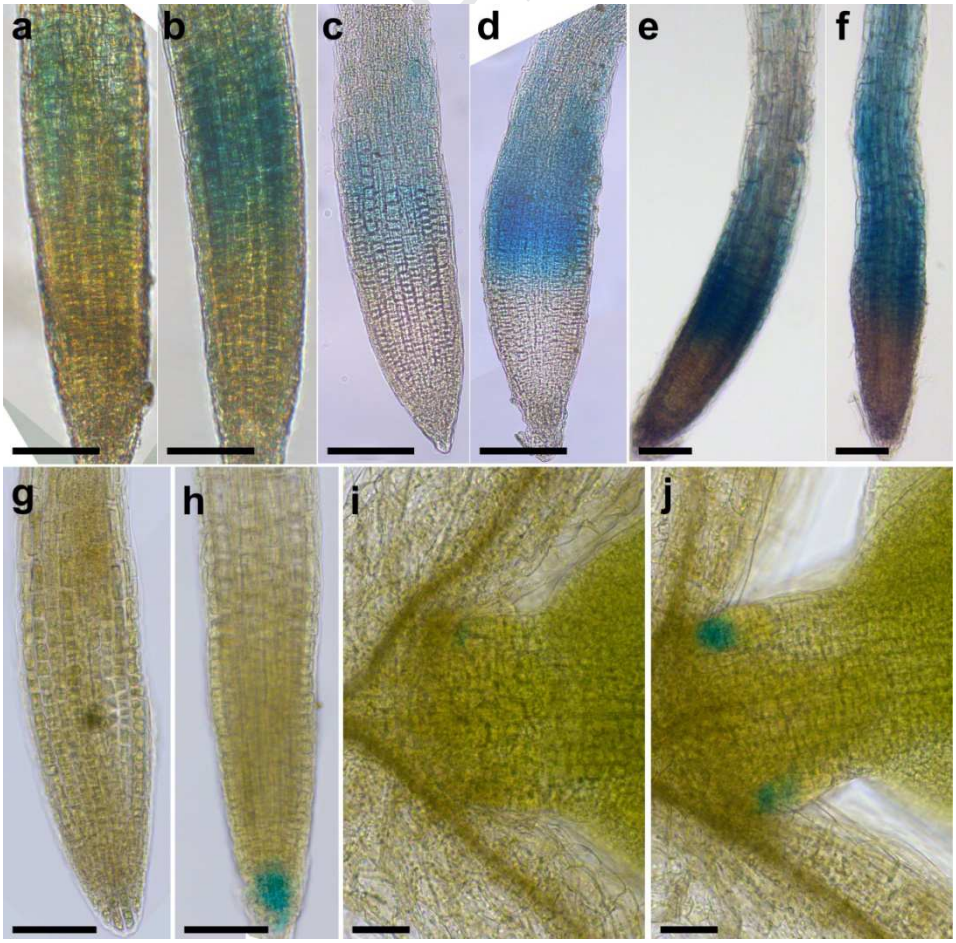

Figure 14. Analysis of *AtCuAOγ1* and *AtCuAOγ2* tissue specific expression pattern upon IAA, ABA and SA treatments.

3.10. Expression profile of *AtCuAOγ1* and *AtCuAOγ2* after dehydration/recovery and wounding stress

As for the case of clade I genes, we investigated the eventual correlation between the *AtCuAOγ1* and *AtCuAOγ2* gene expression profiles after ABA and MeJA treatments with the expression profile of these genes after the abiotic stresses signaled by the same hormones. Specifically, the variations of *AtCuAOγ1* and *AtCuAOγ2* gene expression profiles under dehydration and successive recovery, and upon leaf wounding (Fig. 15) were analyzed.

The applied dehydration stress caused no relevant change in expression levels for *AtCuAOγ1* (Fig. 15, inset in left upper panel) while it strongly repressed *AtCuAOγ2* (40% of T0; Fig. 15, inset in right upper panel). The effects of DR caused significant changes in the expression profiles of both genes. In the case of *AtCuAOγ1*, a peak of 2-fold was observed at T3 time point (3 h DR) followed by a gradual return to T0 levels (Fig. 15, left panel), while for *AtCuAOγ2*, a peak of 1.6 fold was observed at T2 that was followed by a steady reduction towards the last time point (T5, 24 h DR) when a 50% repression was observed. Leaf wounding presented regulation profiles with stronger inductions of both *AtCuAOγ1* and *AtCuAOγ2* expression in respect to those observed in the case of dehydration and recovery stress. In fact, *AtCuAOγ1* expression was induced stably from 3 to 24 h, with 2.7-, 1.7- and 2-fold increases respectively (Fig. 15, lower left panel) and *AtCuAOγ2* presented induced expression at 1 and 3 h (2-fold) returning at 6 h to T0 levels (Fig. 15, lower right panel).

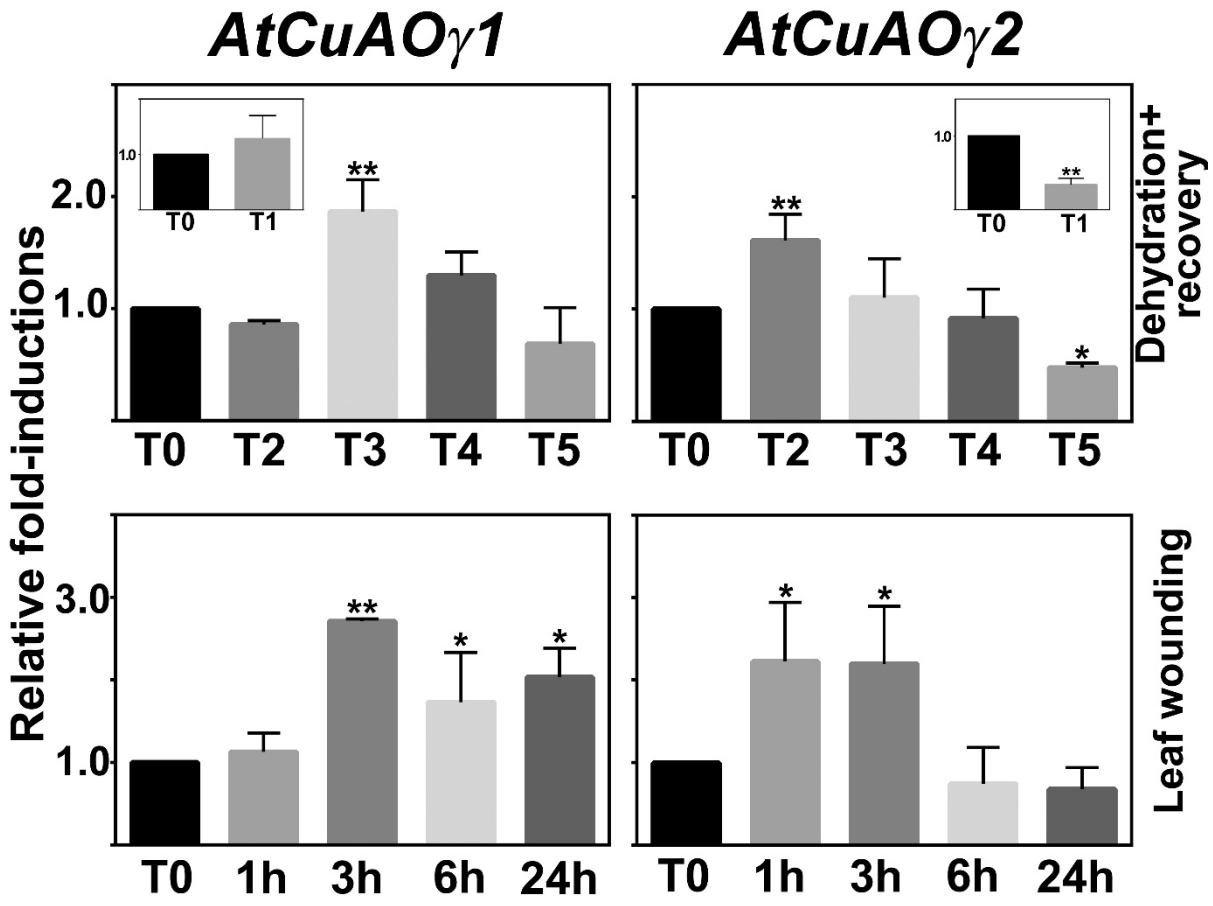

Figure 15. Time-course analysis *AtCuAOγ1* and *AtCuAOγ2* gene expression by RT-qPCR upon abiotic stress treatments (dehydration and recovery and leaf wounding).

Considering the data from RT-qPCR, the analysis of the tissue-specific expression pattern of *AtCuAOγ1* and *AtCuAOγ2* after these stress treatments have been carried out (Fig. 16a-l). Both DR and wounding induced *AtCuAOγ1* expression in the apex/petiole junction after 3 h (Fig. 16b, DR and 16c, leaf wounding) and in the root elongation zone after 6 h (Fig. 16e, DR) and 3 h (Fig. 16f, leaf wounding) when compared to the respective zones of control untreated plants (Fig. 16a and d). *AtCuAOγ2* expression was only induced upon wounding stress (Fig. 16g-l). Expression in the cotyledon apical hydathode (Fig. 16j), stipules of young leaves (Fig. 16k) and the root cap (Fig. 16l) was increased as compared to control untreated plants (Fig. 16g-i).

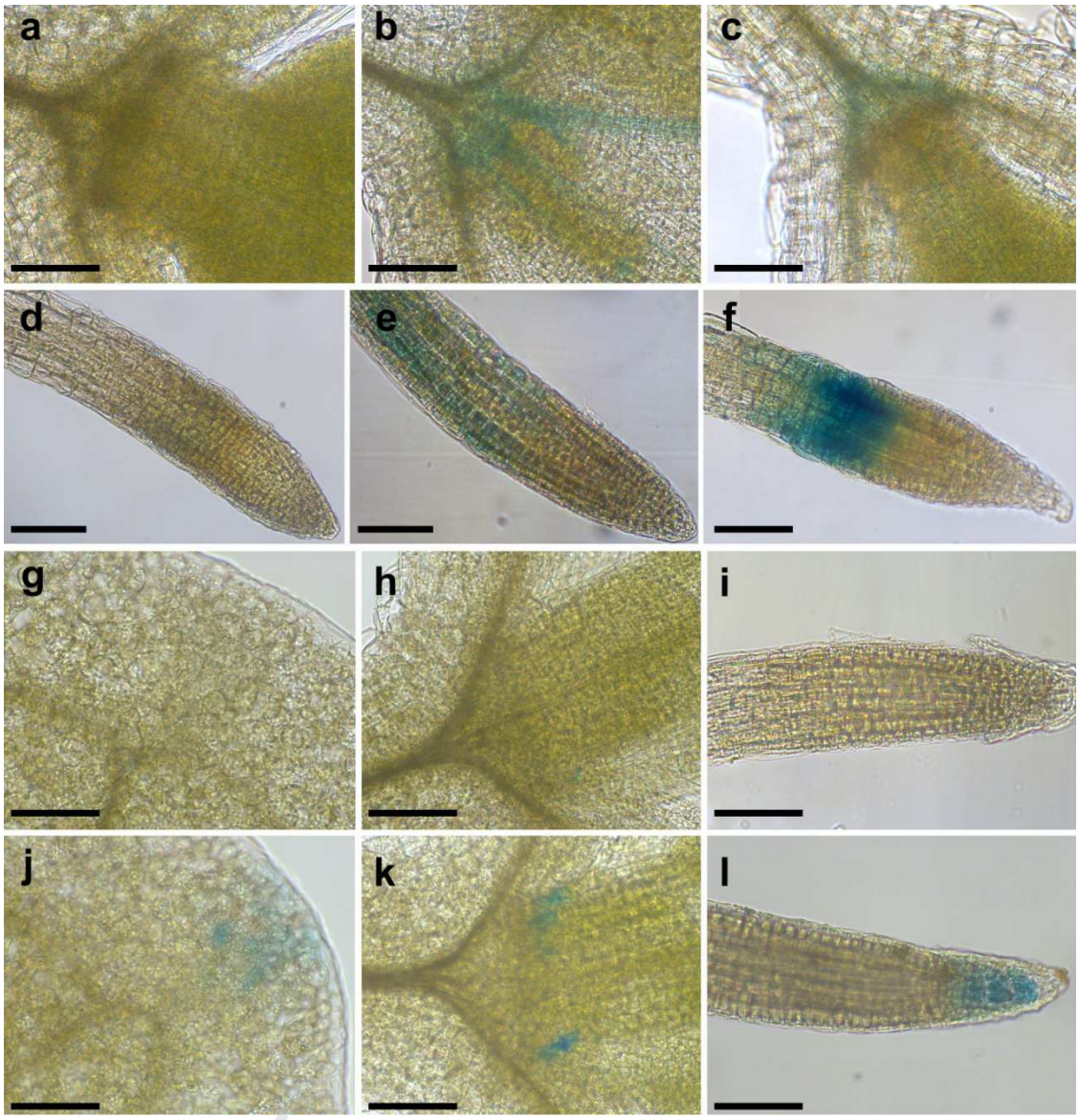

Figure 16. Analysis of *AtCuAOγ1* and *AtCuAOγ2* tissue specific expression pattern upon abiotic stress (cotyledonary leaf wounding and dehydration recovery) treatments.

3.11. Expression profile of *AtCuAOγ1* and *AtCuAOγ2* after treatment with PAs

Following the analysis of the effects of Put and Spd on the expression of the clade I genes, the effects of these PAs on expression of clade II members, *AtCuAOγ1* and *AtCuAOγ2* was studied. These two PAs had diverse effects on the expression of these genes (Fig. 17).

Treatment with 500 µM Put induced both *AtCuAOγ1* and *AtCuAOγ2* expression at similar levels from 1 h up to 3 h (2- to 3-fold). From this time point, expression of *AtCuAOγ1* was maintained at an induced level of approximately 3- and 2-fold, respectively at 6 and 24 h, compared to T0 levels (Fig. 17, upper left panel) while at the same time points *AtCuAOγ2* expression returned

to T0 levels (Fig. 17, upper right panel). The 500 µM Spd treatment responses presented an opposite pattern with visible repression of *AtCuAOγ1* expression at 1 and 3 h (approximately 40% and 50% of T0 respectively; Fig. 17, lower left panel) and no observed significant differences as compared to T0 in the case of *AtCuAOγ2* (Fig. 17, lower right panel).

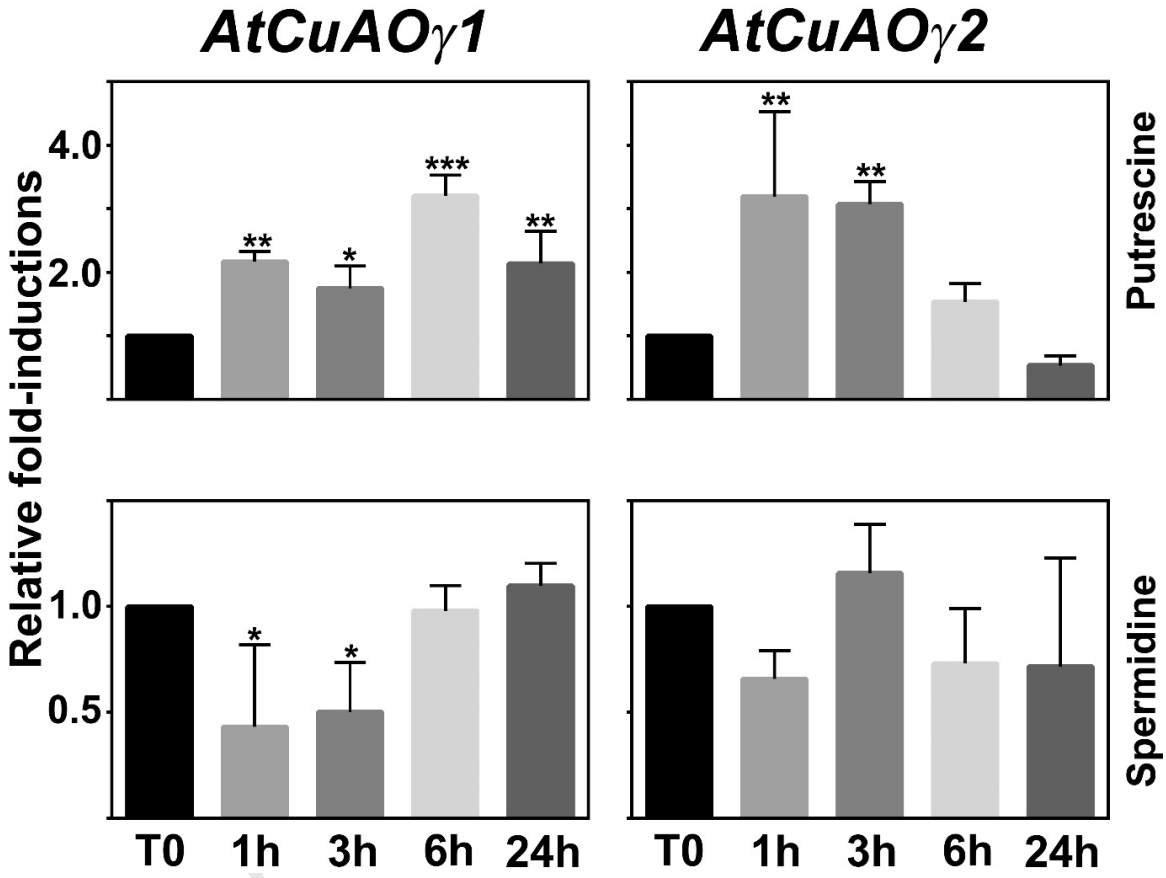

Figure 17. Time-course analysis of *AtCuAOγ1* and *AtCuAOγ2* gene expression by RT-qPCR upon treatment with the polyamines putrescine e spermidine.

Considering data from RT-qPCR, the analysis of the tissue-specific expression pattern of *AtCuAOγ1* and *AtCuAOγ2* after Put treatments has been carried out (Fig. 18). In detail, Put induced *AtCuAOγ1* expression in the stipules, hydathodes of new emerging leaves and root elongation zone (Fig. 18a-d), as revealed by the presence of an intense GUS staining in these tissues (Fig. 18b and d) in comparison to control untreated plants (Fig. 18a and c). Furthermore, Put induced *AtCuAOγ2* expression (Fig. 18e-h) in the cotyledon apical hydathodes and root columella (Fig. 18f and h), as shown by the tissue-specific increase of the promoter-driven GUS expression in Put-treated *AtCuAOγ2-promoter::GFP-GUS* plants as compared to control untreated plants (Fig. 18e and g).

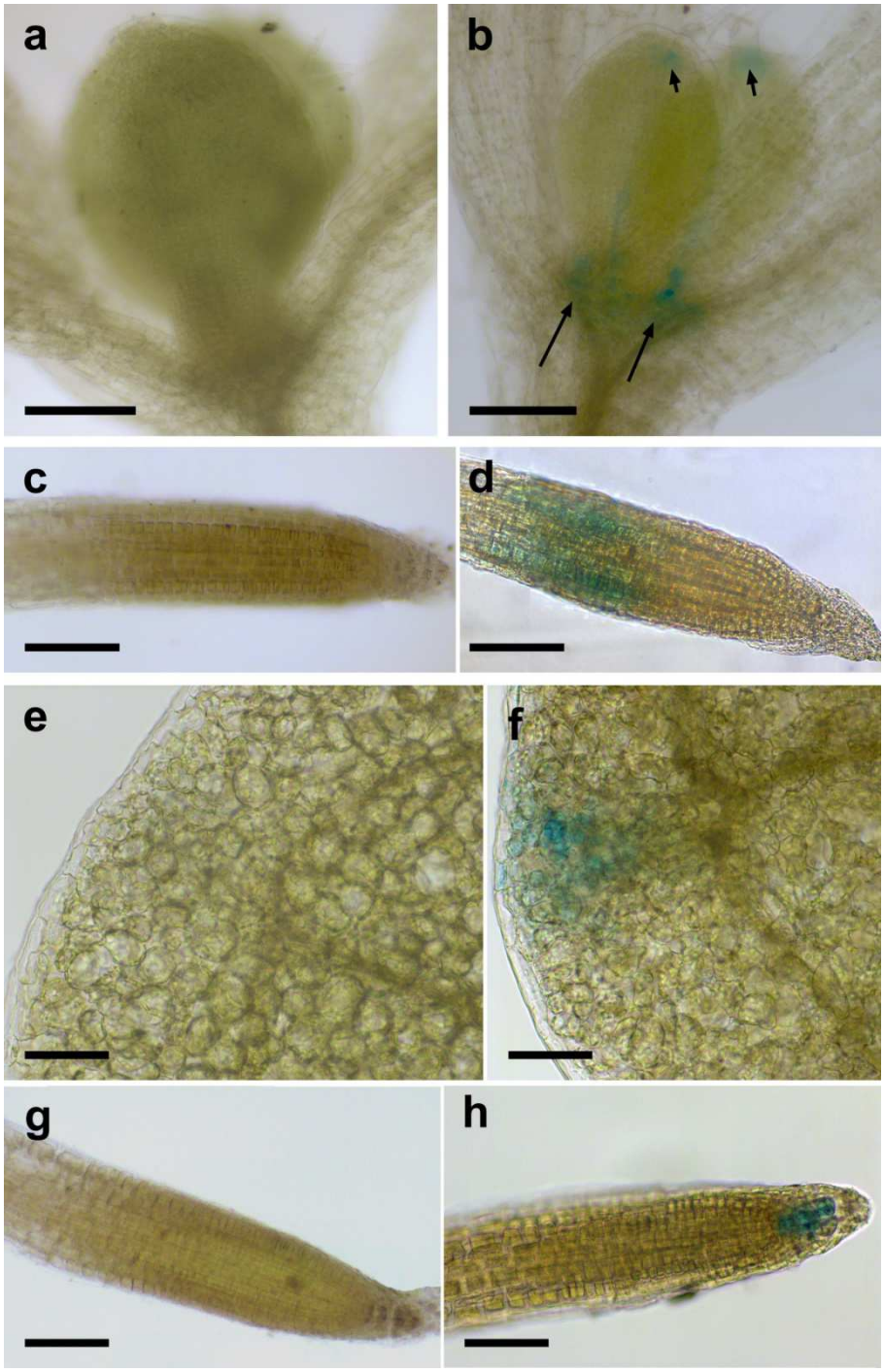

Figure 18. Analysis of *AtCuAOγ1* and *AtCuAOγ2* tissue specific expression pattern upon putrescine treatment.

4. Discussion

4.1. *AtCuAOα2/α3* and *AtCuAOγ1/γ2* gene expression: possible relevance in water balance, vascular tissue differentiation, wounding and immune response

The expression pattern of *AtCuAOα2*, *α3*, *γ1* and *γ2* revealed by GUS staining shows an association with tissues and cells involved in water supply and water loss such as vascular tissues

and hydathodes. In detail, in developing seedlings promoter-driven GUS expression was clearly visible in hydathodes of cotyledons (*AtCuAOα2*, *AtCuAOγ1* and *AtCuAOγ2*; Fig. 1, 4, 7 and 8) and new emerging leaves (*AtCuAOγ1* and *AtCuAOγ2*; Fig. 4, 7 and 8), as well as in vascular tissues of new emerging leaves (*AtCuAOγ1*; Fig. 4 and 7) and hypocotyl/root zones (*AtCuAOα3*; Fig. 2).

In this regard, the occurrence of AOs in tissues involved in water balance homeostasis has been revealed in several plant species. In detail, some AO members have been shown to be expressed in vascular tissues of *Fabacee*, *Poacee* and *Nicotiana tabacum* (Paschalidis et al., 2005; Ghuge et al., 2015c), in stomata of *Vicia faba* (An et al., 2008; Qu et al., 2014), and in both stomata and vascular tissues of Arabidopsis (Kim et al., 2014; Qu et al., 2014; Ghuge et al., 2015a; Ghuge et al., 2015b; Ghuge et al., 2015c; Alabdallah et al., 2017) and *Vitis vinifera* (Paschalidis et al., 2009; Paschalidis et al., 2010). The expression of *AtCuAOα2/α3* and *AtCuAOγ1/γ2* in both stomata-related hydathode pores and vascular tissues, as well as their regulation by DR stress (Fig. 9, 10, 15, 16) is therefore congruent with the previously reported AO localization in tissues and cells involved in water transport, further supporting the hypothesis of an AO role in water balance regulation. Moreover, peroxisomal AtCuAOα3 is likely involved in IAA-induced root xylem differentiation (Fig. 8), although this latter phenomenon may be further regulated by thermospermine and its metabolism by other AOs (Yoshimoto et al., 2016; Alabdallah et al., 2017). On the other hand, *AtCuAOγ1* encoding an apoplastic protein is positively regulated by IAA and shows a strong expression in vascular tissues of young leaves (Fig. 3 and Fig. 13).

It has been shown that both apoplastic and peroxisomal CuAOs and PAOs contribute to the ABA-induced ROS biosynthesis leading to stomatal closure possibly in cooperation with NADPH oxidases (An et al., 2008; Paschalidis et al., 2010; Wimalasekera et at., 2011; Qu et al., 2014). The complex network of ROS sources is further enriched by the recent discovery that the vacuolar AtCuAOδ is involved in the H_2O_2 production related to ABA-induced stomatal closure (Fraudentali et al., 2019). Furthermore, apoplastic PAOs and CuAOs have been involved in early xylem differentiation especially under stress-like conditions, such as those signaled by MeJA treatment

(Ghuge et al., 2015a; Ghuge et al., 2015c) or simulated by treatment with exogenous PAs, AO overexpression (Tisi et al., 2011a; Tisi et al., 2011b) or a compromised status of cell-wall pectin integrity (Cona et al., 2014). Thus, the ROS signature occurring during specific developmental events or in response to biotic/abiotic stress conditions is generated by a complex interplay among AOs with different subcellular localization and possibly NADPH oxidases (Gupta et al., 2016). On this basis, it is reasonable to hypothesize that the peroxisomal *AtCuAOα3* may cooperate with the apoplastic *AtCuAOβ*, both positively regulated by MeJA (Ghuge et al., 2015a) in a potentially MeJA-signaled maturation of root metaxylem vessels (Fig. 2). Therefore, the occurrence of CuAOs with different subcellular localization, tissue specific expression and hormone responsiveness, such as AtCuAOα3 in vascular bundles, the apoplastic ABA- and SA-induced AtCuAOγ1 in vascular tissues of new emerging leaves and the apoplastic AtCuAO*γ2* in vascular bundles of cotyledons, may contribute to developmentally-regulated or stress-induced xylem tissue maturation in these organs. Furthermore, the expression of *AtCuAOα2*, *AtCuAOγ1* and *AtCuAOγ2* in hydathodes, which are structures evolutionarily related to the stoma and represent sites of high free-auxin levels driving xylem differentiation (Aloni et al., 2003), may have a role in xylem maturation of differentiating vascular bundle in cotyledon and leaf. In this context, based on the evidence that *AtCuAOα2* and *AtCuAOα3* expression is induced by the wound associated signal MeJA, we can hypothesize that the encoded CuAOs may have a role in xylem differentiation during the auxin-driven xylem regeneration around a wound (Aloni, 2001). Moreover, it is interesting to note that *AtCuAOγ1/γ2* are positively regulated by wounding but insensitive to MeJA suggesting the involvement of these genes in the MeJA-independent wounding-response pathway (Titarenko et al., 1997; León et al., 1998).

The expression of *AtCuAOα2* and *AtCuAOγ1/γ2* in the hydathodes may be also relevant in the early stage of immune responses. In fact, it has been reported that FLS2 (Flagellin Sensitive2) receptor is expressed in the hydathodes (Beck et al., 2014) and may contribute to ROS production elicited by the bacterial Pathogen Associated Molecular Pattern flagellin (Mersmann et al., 2010).

The apoplastic (AtCuAOγ1) and the peroxisomal (AtCuAOζ) have been already suggested to be involved in flagellin signal transduction (Planas-Portell et al., 2013) and the present data further enrich this *scenario*.

4.2. *AtCuAOα2/α3* and *AtCuAOγ1/γ2* gene expression: possible relevance in PA homeostasis, cell wall maturation, cell expansion and root gravitropism

A combined approach of GUS staining in tissue sections and promoter-driven GFP signal analysis revealed gene expression also in the epidermis of cotyledon and young leaf (*α2*), in the root cortex at the division/elongation transition zone (*γ1*) as well as in cotyledon margins and columella cells (*γ2*). In this regard, AOs have been involved in growth and developmental processes in several plant species. Specifically, apoplastic AOs have been implicated in cell wall maturation events during developmentally-regulated or light-induced tissue differentiation in *Nicotiana tabacum* as well as in species belonging to *Fabaceae* and *Poaceae* (Cona et al., 2006; Kärkönen & Kuchitsu, 2015; Tavladoraki et al., 2016). In these processes, the PA-derived H_2O_2 behaved as a co-substrate in the peroxidase-mediated cross-linking of cell wall polymers and/or lignin/suberin biosynthesis (Angelini et al., 2010). Moreover, it has been suggested that both apoplastic and/or cytosolic H_2O_2 might modulate cell water uptake by regulating the aquaporin abundance at the plasma membrane via endocytosis activation resulting in a reduced water transport (Schmidt et al., 2016). The reduced water uptake hinders the turgor pressure-driven cell expansion cooperating with the cell growth inhibition triggered by wall stiffening events. Taking in mind this consideration, the occurrence of the apoplastic AtCuAOγ1 in outer-tissues (root cortex) of the transition/elongation zones, suggests a role in cell wall stiffening events occurring when cells stop dividing and enter the elongation phase, prior to acquiring a final differentiated status. Likewise, the expression of the peroxisomal AtCuAOα2 in the growth-rate controlling epidermis of cotyledon and young leaf, might contribute through aquaporin activity modulation to the inhibition of the cell growth eventually triggered by a cell wall localized production of H_2O_2.

Interestingly, *AtCuAOγ2* is specifically expressed in columella cells and is positively regulated by IAA, suggesting a possible link with gravitropic response through an AO-mediated H_2O_2-dependent negative regulatory loop (Su et al., 2017; Zhou et al., 2018).

On the other hand, since the simultaneous production of H_2O_2 and superoxide anion (O_2^{-}) leads to the enzymatic or chemical formation of the wall-loosening agent hydroxyl radical ($OH^{\cdot}$), the H_2O_2 derived from AO-mediated PA oxidation could thus participate in the ROS-mediated cell-wall expansion, depending on a specific ROS signature (Gupta et al. 2016; Schmidt et al., 2016). In line with this hypothesis, the soybean CuAO-driven H_2O_2 production has been involved in cell expansion of fast-growing tissues (Delis et al., 2006). In this context it is interesting to note that *AtCuAOα2* and *AtCuAOγ1* are positively regulated by IAA in fast expanding tissues of leaf primordia and root elongation zone their encoded products possibly contributing to H_2O_2 biosynthesis needed for wall expansion (Fig. 1, 3, 7, 8, 13, 14).

Furthermore, ROS have also been involved in meristem size specification by controlling the transition between cell proliferation and differentiation, independently from the cytokinin/auxin pathway (Bishopp et al., 2011; Petricka et al., 2012), with H_2O_2 and $O_2^{-\cdot}$ respectively promoting cell differentiation and cell division (Tsukagoshi et al., 2010). In this regard, it is worth mentioning that analysis of *AtCuAOα2, α3, γ1* and *γ2* expression pattern reveals overlapping profiles both to each other and in relation to the tissue distribution pattern of free-auxin production sites (Aloni et al., 2003; Jacobs & Roe, 2005), suggested to control basipetal maturation sequences and vascular differentiation in leaf and root (Aloni et al., 2003; Petricka et al., 2012). In detail, among the free-auxin production sites a specific expression profile of each of the analyzed members of the *AtCuAO* family has been displayed: *AtCuAOα3* is expressed in stipules; *α2* and *γ1* in leaf primordium tip; *α2, γ1* and *γ2* in hydathodes; *α2* in leaf margins; *γ2* and *AtCuAOβ* (Ghuge et al., 2015a) in root apex; *AtCuAOβ* (Ghuge et al., 2015a) in the youngest region of the differentiating central cylinder and *AtCuAOβ* (Ghuge et al., 2015c) and *AtCuAOζ* (Qu et al., 2014) in stomata. The occurrence of AtCuAO family members in each of the zones where an auxin maximum has been observed support

the above reported evidences of CuAO roles in tissue maturation events and xylem differentiation, especially under stress conditions, by leading to H_2O_2 production consequent to the modulation of *AtCuAO* gene expression and PA homeostasis and transport. In this regard, the positive regulation by Put of the expression of *CuAO* genes under study may represent the necessity of a fine PA homeostasis and/or a mechanism for H_2O_2 production (Fig. 11, 12, 17, 18). Indeed, it is known that at specific developmental stages or under stress conditions, the H_2O_2 derived by the CuAO-driven PA-oxidation may trigger both wall maturation events and induction of defense- and developmental programmed cell death (PCD)-gene expression (Ghuge et al., 2015c).

Funding

This work was supported by the Grant of Excellence Departments, Italian Ministry for University and Research (MIUR-ARTICOLO 1, COMMI 314 – 337 LEGGE 232/2016; Italy), (I.F., S.G., A.C.a., R.A., P.T., and A.C.,), the Progetti di Ricerca di Interesse Nazionale (PRIN) 2017 (project contract no. 2017ZBBYNC_002 to R.A.) of the Ministero dell'Istruzione, dell'Università e della Ricerca (MIUR, Italy) and the Project "Ricerca d'Interesse d'Ateneo"-RIA 2015, RIA 2016, RIA 2017, and RIA 2018 from the Università dell'Aquila-Department of Life, Health, and Environmental Sciences, Italy (RAR-P).

Contributions

AC and RA conceived the project. SG, RAR-P and AC designed the study. IF, SG, and ACa performed most of the experiments. All the authors contributed to data analysis. RAR-P and AC wrote the manuscript with contributions of RA, PT and the other authors.

Acknowledgements

The authors would like to thank Eleonora Vertecchi and Micaela Donnini for their extremely helpful contribution in performing all the histochemical sections and image acquisitions necessary for the promoter-GUS analysis used in this work.

References

Ahou A, Martignago D, Alabdallah O, Tavazza R, Stano P, Macone A, Pivato M, Masi A, Rambla JL, Vera-Sirera F, Angelini R, Federico R, Tavladoraki P. A plant spermine oxidase/dehydrogenase regulated by the proteasome and polyamines. J Exp Bot. 2014, 65:1585-1603.

Alabdallah O, Ahou A, Mancuso N, Pompili V, Macone A, Pashkoulov D, Stano P, Cona A, Angelini R, Tavladoraki P. The Arabidopsis polyamine oxidase/dehydrogenase 5 interferes with cytokinin and auxin signaling pathways to control xylem differentiation. J Exp Bot. 2017, 68:997-1012.

Aloni R. Foliar and axial aspects of vascular differentiation: hypotheses and evidence. J Plant Growth Regul. 2001, 20:22–34.

Aloni R, Schwalm K, Langhans M, Ullrich CI. Gradual shifts in sites of free-auxin production during leaf-primordium development and their role in vascular differentiation and leaf morphogenesis in Arabidopsis. Planta 2003, 216:841–53.

An Z, Jing W, Liu Y, Zhang W. Hydrogen peroxide generated by copper amine oxidase is involved in abscisic acid-induced stomatal closure in Vicia faba. J Exp Bot. 2008, 59:815–25.

Angelini R, Cona A, Federico R, Fincato P, Tavladoraki P, Tisi A. Plant amine oxidases “on the move”: An update. Plant Physiol Biochem. 2010, 48:560–4.

Beck M, Wyrsch I, Strutt J, Wimalasekera R, Webb A, Boller T, Robatzek S. Expression patterns of FLAGELLIN SENSING 2 map to bacterial entry sites in plant shoots and roots. J Exp Bot. 2014, 65:6487–98.

Berta G, Altamura MM, Fusconi A, Cerruti F, Capitani F, Bagni N. The plant cell wall is altered by inhibition of polyamine biosynthesis. New Phytol. 1997, 137:569-77.

Bishopp A, Help H, El-Showk S, Weijers D, Scheres B, Friml J, Benková E, Mähönen AP, Helariutta Y. A mutually inhibitory interaction between auxin and cytokinin specifies vascular pattern in roots. Curr Biol. 2011, 21:917–26.

Boudart G, Jamet E, Rossignol M, Lafitte C, Borderies G, Jauneau A, Esquerré-Tugayé MT, Pont-Lezica R. Cell wall proteins in apoplastic fluids of Arabidopsis thaliana rosettes: identification by mass spectrometry and bioinformatics. Proteomics 2005, 5:212–21.

Cai G, Sobieszczuk□Nowicka E, Aloisi I, Fattorini L, Serafini-Fracassini D, Del Duca S. Polyamines are common players in different facets of plant programmed cell death. Amino Acids 2015, 47:27–44.

Carter C, Pan S, Zouhar J, Avila EL, Girke T, Raikhel NV. The vegetative vacuole proteome of Arabidopsis thaliana reveals predicted and unexpected proteins. Plant Cell 2004, 16:3285-303.

Clough SJ and Bent AF. Floral dip: a simplified method for Agrobacterium-mediated transformation of Arabidopsis thaliana. Plant J. 1998, 16:735-43.

Cona A, Rea G, Angelini R, Federico R, Tavladoraki P. Functions of amine oxidases in plant development and defence. Trends Plant Sci. 2006, 11:80–88.

Cona A, Tisi A, Ghuge SA, Franchi S, de Lorenzo G, Angelini R. Wound healing response and xylem differentiation in tobacco plants over-expressing a fungal endopolygalacturonase is mediated by copper amine oxidase activity. Plant Physiol Biochem. 2014, 82:54–65.

Czechowski T, Stitt M, Altmann T, Udvardi MK. Genome-Wide Identification and Testing of Superior Reference Genes for Transcript Normalization. Plant Physiol. 2005, 139:5–17.

Delis C, Dimou M, Flemetakis E, Aivalakis G, Katinakis P. A root- and hypocotyl-specific gene coding for copper-containing amine oxidase is related to cell expansion in soybean seedlings. J Exp Bot. 2006, 57:101-11.

Fincato P, Moschou PN, Spedaletti V, Tavazza R, Angelini R, Federico R, Roubelakis-Angelakis KA, Tavladoraki P. Functional diversity inside the Arabidopsis polyamine oxidase gene family. J Exp Bot. 2011, 62:1155–68.

Fincato P, Moschou PN, Ahou A, Angelini R, Roubelakis-Angelakis K A, Federico R. The members of Arabidopsis thaliana PAO gene family exhibit distinct tissue-andorgan-specific expression pattern during seedling growth and flower development. Amino Acids 2012, 42:831–41.

Fraudentali I, Ghuge SA, Carucci A, Tavladoraki P, Angelini R, Cona A, Rodrigues-Pousada RA. The copper amine oxidase AtCuAOδ participates in abscisic acid-induced stomatal closure in Arabidopsis. Plants (Basel) 2019, 8:E183, doi: 10.3390/plants8060183.

Fukao Y, Hayashi M, Hara-Nishimura I, Nishimura M. Novel glyoxysomal protein kinase, GPK1, identified by proteomic analysis of glyoxysomes in etiolated cotyledons of Arabidopsis thaliana. Plant Cell Physiol. 2003, 44:1002-12.

Fulton TM, Chunwongse J, Tanksley SD. Microprep Protocol for Extraction of DNA from Tomato and other Herbaceous Plants. Plant Mol Biol Report. 1995, 13:207-9.

Ghuge SA, Carucci A, Rodrigues Pousada RA, Tisi A, Franchi S, Tavladoraki P, Angelini R, Cona A. The apoplastic copper AMINE OXIDASE1 mediates jasmonic acid-induced protoxylem differentiation in Arabidopsis roots. Plant Physiol. 2015a, 168:690–707.

Ghuge SA, Carucci A, Rodrigues-Pousada RA, Tisi A, Franchi S, Tavladoraki P, Angelini R, Cona A. The MeJA-inducible copper amine oxidase AtAO1 is expressed in xylem tissue and guard cells. Plant Signal Behav. 2015b, 10:1073872.

Ghuge SA, Tisi A, Carucci A, Rodrigues-Pousada RA, Franchi S, Tavladoraki P, Angelini R, Cona A. Cell Wall Amine Oxidases: New Players in Root Xylem Differentiation under Stress Conditions. Plants 2015c, 4:489-504.

Groß F, Rudolf EE, Thiele B, Durner J, Astier J. Copper amine oxidase 8 regulates arginine-dependent nitric oxide production in Arabidopsis thaliana. J Exp Bot. 2017, 68:2149-62.

Gupta K, Sengupta A, Chakraborty M, Gupta B. Hydrogen Peroxide and Polyamines Act as Double Edged Swords in Plant Abiotic Stress Responses. Front Plant Sci. 2016, 7:1343.

Jacobs J, Roe JL. SKS6, a multicopper oxidase-like gene, participates in cotyledon vascular patterning during Arabidopsis thaliana development. Planta 2005, 222:652–66.

Jefferson RA. Assaying chimeric genes in plants: the GUS gene fusion system. Plant Mol Biol. 1987, 5:387–405.

Jiménez-Bremont JF, Marina M, Guerrero-González Mde L, Rossi FR, Sánchez-Rangel D, Rodríguez-Kessler M, Ruiz OA, Gárriz A. Physiological and molecular implications of plant polyamine metabolism during biotic interactions. Front Plant Sci. 2014, doi: 10.3389/fpls.2014.00095.

Kärkönen A, Kuchitsu K. Reactive oxygen species in cell wall metabolism and development in plants. Phytochemistry 2015, 112, 22–32.

Kim DW, Watanabe K, Murayama C, Izawa S, Niitsu M, Michael AJ, Berberich T, Kusano T. Polyamine oxidase 5 regulates Arabidopsis growth through thermospermine oxidase activity. Plant Physiol. 2014, 165:1575–90.

Kumar V, Dooley DM, Freeman HC, Guss JM, Harvey I, McGuirl MA, Wilce MC, Zubak VM. Crystal structure of a eukaryotic (pea seedling) copper-containing amine oxidase at 2.2 □ resolution. Structure 1996, 4:943–55.

León J, Rojo E, Titarenko E, Sánchez-Serrano JJ. Jasmonic acid-dependent and -independent wound signal transduction pathways are differentially regulated by Ca2+/calmodulin in Arabidopsis thaliana. Mol Gen Genet. 1998, 258:412-9.

Livak KJ, Schmittgen TD. Analysis of relative gene expression data using real-time quantitative PCR and the 2 (Delta Delta C(T)) Method. Methods 2001, 25:402–8.

Mattoo AK, Sobolev AP, Neelam A, Goyal RK, Handa AK, Segre AL. Nuclear magnetic resonance spectroscopy-based metabolite profiling of transgenic tomato fruit engineered to accumulate spermidine and spermine reveals enhanced anabolic and nitrogen–carbon interactions. Plant Physiol. 2006, 142:1759–70.

Mersmann S, Bourdais G, Rietz S, Robatzek S. Ethylene signaling regulates accumulation of the FLS2 receptor and is required for the oxidative burst contributing to plant immunity. Plant Physiol. 2010, 154:391-400.

Minocha R, Majumdar R, Minocha SC. Polyamines and abiotic stress in plants: a complex relationship. Front Plant Sci. 2014, 5:175.

Møller SG, McPherson MJ. Developmental expression and biochemical analysis of the Arabidopsis atao1 gene encoding an H_2O_2-generating diamine oxidase. The Plant J. 1998, 13:781–91.

Moschou PN, Paschalidis KA, Delis ID, Andriopoulou AH, Lagiotis GD, Yakoumakis DI, Roubelakis-Angelakis KA. Spermidine exodus and oxidation in the apoplast induced by abiotic stress is responsible for H_2O_2 signatures that direct tolerance responses in tobacco. Plant Cell 2008, 20:1708-24.

Moschou PN, Wu J, Cona A, Tavladoraki P, Angelini R, Roubelakis-Angelakis KA. The polyamines and their catabolic products are significant players in the turnover of nitrogenous molecules in plants. J Exp Bot. 2012, 63:5003–15.

Moschou PN, Roubelakis-Angelakis KA. Polyamines and programmed cell death. J Exp Bot. 2014, 65:1285-96

Murray-Stewart TR, Woster PM, Casero RA Jr. Targeting polyamine metabolism for cancer therapy and prevention. Biochem J. 2016, 473:2937-53.

Naconsie M, Kato K, Shoji T, Hashimoto T. Molecular evolution of N-methylputrescine oxidase in tobacco. Plant Cell Physiol. 2014, 55:436–44.

Nakagawa T, Kurose T, Hino T, Tanaka K, Kawamukai M, Niwa Y, Toyooka K, Matsuoka K, Jinbo T, Kimura T. Development of series of gateway binary vectors, pGWBs, for realizing efficient construction of fusion genes for plant transformation. J Biosci Bioeng. 2007, 104:34-41.

Paschalidis KA, Roubelakis-Angelakis KA. Sites and regulation of polyamine catabolism in the tobacco plant. Correlations with cell division/expansion, cell cycle progression and vascular development. Plant Physiol. 2005, 138:2174-84.

Paschalidis KA, Moschou PN, Toumi I, Roubelakis-Angelakis KA. Polyamine anabolic/catabolic regulation along the woody grapevine plant axis. J Plant Physiol. 2009, 166:1508-19.

Paschalidis KA, Toumi I, Moschou PN, Roubelakis-Angelakis KA. ABA-dependent amine oxidases-derived H_2O_2 affects stomata conductance. Plant Signal Behav. 2010, 5:1153–56.

Petricka JJ, Winter CM, Benfey PN. Control of Arabidopsis root development. Annu Rev Plant Biol. 2012, 63:563–90.

Planas-Portell J, Gallart M, Tiburcio AF, Altabella T. Copper containing amine oxidases contribute to terminal polyamine oxidation in peroxisomes and apoplast of Arabidopsis thaliana. BMC Plant Biol. 2013, 13:109–22.

Qu Y, An Z, Zhuang B, Jing W, Zhang Q, Zhang W. Copper amine oxidase and phospholipase D act independently in abscisic acid (ABA)-induced stomatal closure in Vicia faba and Arabidopsis. J Plant Res. 2014, 127:533–44.

Sagor GH, Zhang S, Kojima S, Simm S, Berberich T, Kusano T. Reducing Cytoplasmic Polyamine Oxidase Activity in Arabidopsis Increases Salt and Drought Tolerance by Reducing Reactive Oxygen Species Production and Increasing Defense Gene Expression. Front Plant Sci. 2016, 7:214

Schmidt R, Kunkowska AB, Schippers JH. Role of reactive oxygen species during cell expansion in leaves. Plant Physiol. 2016, 172:2098–106.

Sobieszczuk-Nowicka E. Polyamine catabolism adds fuel to leaf senescence. Amino Acids 2017, 49:49-56.

Su SH, Gibbs NM, Jancewicz AL, Masson PH. Molecular mechanisms of root gravitropism. Curr Biol. 2017, 27:R964-R972.

Tavladoraki P, Cona A, Federico R, Tempera G, Viceconte N, Saccoccio S, Battaglia V, Toninello A, Agostinelli E. Polyamine catabolism: target for antiproliferative therapies in animals and stress tolerance strategies in plants. Amino Acids 2012, 42:411–26.

Tavladoraki P, Cona A, Angelini R. Copper-containing amine oxidases and FAD-dependent polyamine oxidases are key players in plant tissue differentiation and organ development. Front Plant Sci. 2016, 7:824.

Tiburcio AF, Altabella T, Bitrián M, Alcázar R. The roles of polyamines during the lifespan of plants: from development to stress. Planta 2014, 240:1–18.

Tisi A, Angelini R, Cona A. Does polyamine catabolism influence root development and xylem differentiation under stress conditions? Plant Signal Behav. 2011a, 11:1844–47.

Tisi A, Federico R, Moreno S, Lucretti S, Moschou PN, Roubelakis-Angelakis KA, Angelini R, Cona A. Perturbation of polyamine catabolism can strongly affect root development and xylem differentiation. Plant Physiol. 2011b, 157:200–15.

Titarenko E, Rojo E, León J, Sánchez-Serrano JJ. Jasmonic acid-dependent and -independent signaling pathways control wound-induced gene activation in Arabidopsis thaliana. Plant Physiol. 1997, 115:817-26.

Tsukagoshi H, Busch W, Benfey PN. Transcriptional regulation of ROS controls transition from proliferation to differentiation in the root. Cell 2010, 143:606–16.

Valvekens D, Van Montagu M, Van Lijsebettens M. Agrobacterium tumefaciens-mediated transformation of Arabidopsis thaliana root explants by using kanamycin selection. Proc Natl Acad Sci USA. 1988, 85:5536-40.

Verma V, Ravindran P, Kumar PP. Plant hormone-mediated regulation of stress responses. BMC Plant Biol. 2016, 16:86.

Wimalasekera R, Villar C, Begum T, Scherer GFE. COPPER AMINE OXIDASE1 (CuAO1) of Arabidopsis thaliana contributes to abscisic acid- and polyamine-induced nitric oxide biosynthesis and abscisic acid signal transduction. Mol Plant. 2011, 4:663–78.

Winter D, Vinegar B, Nahal H, Ammar R, Wilson GV, Provart NJ. An "Electronic Fluorescent Pictograph" browser for exploring and analyzing large-scale biological data sets. PLoS ONE 2007, 2:718.

Yoda H, Yamaguchi Y, Sano H. Induction of hypersensitive cell death by hydrogen peroxide produced through polyamine degradation in tobacco plants. Plant Physiol. 2003, 132:1973-81.

Yoshimoto K, Takamura H, Kadota I, Motose H, Takahashi T. Chemical control of xylem differentiation by thermospermine, xylemin, and auxin. Sci Rep. 2016, 6:21487, doi: 10.1038/srep21487.

Zarza X, Atanasov KE, Marco F, Arbona V, Carrasco P, Kopka J, Fotopoulos V, Munnik T, Gómez-Cadenas A, Tiburcio AF, Alcázar R. Polyamine oxidase 5 loss-of-function mutations in Arabidopsis thaliana trigger metabolic and transcriptional reprogramming and promote salt stress tolerance. Plant Cell Environ. 2017, 40:527-42.

Zhou L, Hou H, Yang T, Lian Y, Sun Y, Bian Z, Wang C. Exogenous hydrogen peroxide inhibits primary root gravitropism by regulating auxin distribution during Arabidopsis seed germination. Plant Physiol Biochem. 2018, 128:126-133.

Figure legends

Fig. 1 *AtCuAOα2* tissue expression pattern in 3- (a-d), 5- (e-k) and 7-day-old (l-n) *AtCuAOα2-promoter::GFP-GUS* Arabidopsis transgenic seedlings by light microscopy analysis after GUS staining (a-h; l-n) and LSCM analysis of GFP signal (i-k). **a**, 3-day-old whole seedling. **b-d** Magnified details of GUS staining in 3-day-old seedlings showing cotyledon with diffused GUS staining particularly strong in apical hydathode (b, c) and shoot apex with clear staining at the tip of one of the leaf primordia (d; Lp). **e** 5-day-old whole seedling. **f-h** Details of GUS staining in 5-day-old seedlings. Strongly stained cotyledon and newly emerging leaf (f); stained hydathode and surrounding tissues (g); emerging leaf with staining in its apical part (h). **i-k** GFP fluorescence in 5-day-old seedlings. GFP fluorescence in the epidermal layer of a cotyledon (i); and sub-epidermal layer neighboring the hydathode (j); GFP signal associated with young leaf margins (k). **l-n** Details of GUS staining in 7-day-old seedlings. Cotyledon with spotted staining and the strongly stained hydathode (l); magnification of apical hydathode of cotyledon presented in **l** (m); shoot apex with expanding first leaves showing strong staining (n). GUS staining reaction proceeded overnight.
a, Bar = 500 µm; b, d, h, Bar = 100 µm; c, g, i, m, Bar = 50 µm; e, Bar = 1 mm; f, l, n, Bar = 200 µm; j, k, Bar = 25 µm.

Fig. 2 *AtCuAOα3* tissue expression pattern in 3- (a-e), 5- (f-o) and 7-day-old (p-s) *AtCuAOα3-promoter::GFP-GUS* transgenic seedlings and sections by light microscopy analysis after GUS staining. **a** 3-day-old whole seedling. **b-e** Details of GUS staining in 3-day-old seedlings. Shoot apex showing staining in stipules (b); GUS staining in vascular tissue of hypocotyl (c), hypocotyl/root junction (d), and root mature zone (e). **f** 5-day-old whole seedling. **g-j** Details of GUS staining in 5-day-old seedlings. GUS staining associated with stipules in shoot apex (g), hypocotyl (h), hypocotyl/root junction (i) and vascular tissues of root mature zone (j). **k-o** Details of GUS staining in sections of 5-day-old seedlings. Longitudinal section of shoot apex with details of leaf primordia showing GUS staining in stipules (k); longitudinal section of hypocotyl with promoter activity associated with xylem vessels (l); cross-sections of hypocotyl (m), hypocotyl/root junction (n) and root mature zone (o) showing promoter activity in vascular tissue, remarkably in metaxylem vessels. **p-s** Details of GUS staining in 7-day-old seedlings. Shoot apex with GUS staining in stipules (p, q); GUS staining associated with vascular tissues of hypocotyl/root junction (r) and root (s). Staining reaction proceeded overnight. a, r, s, bar = 500 µm; b, c, d, e, h, i, bar = 100 µm; f, bar = 1 mm; g, j, k, l, n, bar = 50 µm; m, o, q, bar = 25 µm; p, bar = 200 µm.

Fig. 3 *AtCuAOγ1* tissue expression pattern in 3- (a-g), 5- (h-o) and 7-day-old (p-t) *AtCuAOγ1-promoter::GFP-GUS* transgenic seedlings by light microscopy analysis after GUS staining (a-l and p-t) and LSCM analysis of GFP signal (m-o). **a** Three-day-old whole seedling. **b-g** Three-day-old seedlings showing promoter-driven GUS expression in shoot apex (b), apical tip of cotyledon (c), hypocotyl and hypocotyl/root junction (d), mature zone of the root (e) and root division/elongation transition zone (f, g). **h** Five-day-old whole seedling. **i-l** Five-day-old seedlings showing cotyledon apical tip (magnification from **h)** with staining in vascular tissues and hydathode (i); leaf primordia with staining in developing vascular tissues and in the apical tip (j); magnification of leaf primordia shown in **j** with staining clearly associated with developing vascular tissue (k); root apex showing GUS staining of ground tissues starting from the elongation zone towards the differentiation zone (l). **m-o** GFP fluorescence in 5-day-old seedlings. GFP signal in the cortical cell files of the root apex, from the end of the division zone towards the elongation and differentiation zone (m); sequential confocal sections from root epidermis (on the left) to the central zone (on the right)**,** showing GFP signal

associated with cortex cells (n); GFP signal in mature zone of the root with an emerged lateral root (o). **p-t** Details of GUS staining in 7-day-old seedlings. Cotyledon with staining in the apical hydathode (p); expanding leaf with strong expression associated with developing vascular system and hydathodes (q); magnified details of q (r); root mature zones with staining in ground tissues (s, t). GUS staining reaction proceeded overnight. a, p, bar = 500 µm; b, c, d, f, j, o, q, r, bar = 100 µm; e, g, k, l, m, s, t, bar = 50 µm; h, bar = 1 mm; i, bar = 200 µm.

Fig. 4 *AtCuAOγ1* tissue expression pattern in sections of 5-day-old *AtCuAOγ1-promoter::GFP-GUS* transgenic Arabidopsis seedlings by light microscopy analysis after GUS staining. **a** Cross section of cotyledons with expression associated with vascular bundle. **b** Tangential sections of cotyledon upper lamina with staining in vascular bundle. **c** Details of vascular bundle showing staining in vascular tissues. **d** Section of cotyledon with promoter activity in vascular tissues. **e** Magnification of vascular tissue with its associated GUS expression. **f-h** Longitudinal sections of shoot apex in sequence, showing staining associated with the junction of leaf primordia with hypocotyls. **i** Longitudinal root apex section showing GUS staining at the transition/elongation zone. **j** Longitudinal section of root mature zone. **k** Two root cross sections in sequence showing expression associated with ground tissues especially cortical cell layer. *en*: endodermis; *c*: cortex; *p*: pericycle; *v*: vascular tissues. **l** Cross section of hypocotyl above hypocotyl/root junction showing strong GUS expression in vascular tissue. **m** and **n** Longitudinal section of hypocotyl/root junction with strong promoter activity in vascular tissue. **o** Magnification of vascular tissue of hypocotyl/root junction showed in m. **p** Mature root cross section with expression associated with ground tissues. Staining reaction proceeded overnight. a, b, bar = 200 µm; c, d, bar = 100 µm; e-n, p, bar = 50 µm; o, bar = 25 µm.

Fig. 5 *AtCuAOγ2* tissue expression pattern in 3- (a-e), 5- (f-n) and 7-day-old (o-r) *AtCuAOγ2-promoter::GFP-GUS* Arabidopsis transgenic seedlings by light microscopy analysis after GUS staining (a-g; i-l; o-r) and LSCM analysis of GFP signal (h, m, n). **a** 3-day-old whole seedling. **b-e** Details of GUS staining in 3-day-old seedlings. Promoter-driven GUS expression was detectable in hydathode in cotyledon (b), in hypocotyl (c), in root and hypocotyl/root junction (d) and in root apex (e). **f** 5-day-old whole seedling. **g, i, j, k, l** Details of GUS staining in 5-day-old seedlings. Stained hydathode in cotyledons (g); hypocotyl with view of shoot apex (i); GUS staining associated with apical hydathodes in newly formed expanding leaves (j); details of root mature zone close to the hypocotyl/root junction with stained ground tissues (k); strong promoter activity in root apex (l). **h, m, n** GFP fluorescence in 5-day-old seedlings. GFP signal associated with cotyledon margins at hydathodes (h); confocal section of the root tip showing expression clearly associated with columella cells (m); reconstructed projection of a series of confocal sections of the root tip showing GFP signal associated with root cap (n). **o-r** Details of GUS staining in 7-day-old seedlings. Strong promoter activity in fully expanded cotyledon with clearly stained hydathode (o); stained apical hydathodes in newly formed expanding leaves repeating the pattern visible already in 5-day-old seedlings (p); hypocotyl/root junction (q); magnified details of root mature zone, with staining in ground tissues (r). GUS staining reaction proceeded overnight. a, bar = 500 µm; b, k, r, bar = 50 µm; c, d, j, bar= 100 µm; e, h, l, m, n, bar = 25 µm; f, bar = 1 mm; g, i, o, p, q, bar = 200 µm.

Fig. 6 *AtCuAOγ2* tissue expression pattern in sections of 5-day-old *AtCuAOγ2-promoter::GFP-GUS* transgenic seedlings by light microscopy analysis after GUS staining. **a** Longitudinal section of the root tip with appreciable staining in root cap. **b** Cross section of root tip with staining of the whole root cap. **c** and **d** Cross sections of roots with

clearly stained epidermis, cortex and endodermis. **e** and **f** Cross and longitudinal sections of hypocotyl showing GUS staining in epidermal and cortical cell files. **g** Tangential section of upper lamina of cotyledon with associated promoter activity in hydathode zone. **h** Magnified detail of g showing staining of mesophyll cells around the vascular bundle. **i** and **j** Longitudinal sections of shoot apex showing clear staining in the apical zone of leaf primordial. **k** Cotyledon cross section showing strong staining around the central vascular bundle. **l** Magnified details of k, showing the vascular bundle and the strong staining around it. Staining reaction proceeded overnight. a-f, h-j, l, bar = 25 µm; g, k, bar = 100 µm.

Fig. 7 Time-course analysis of *AtCuAOα2* and *AtCuAOα3* gene expression by RT-qPCR upon treatment with IAA (a, b), MeJA (c, d), ABA (e, f) and SA (g, h). Gene expression was analyzed in 7-day-old WT seedlings untreated or treated with 10 µM IAA, 50 µM MeJA, 100 µM ABA or 2mM SA for 0 (T0), 1, 3, 6 and 24 h. The reported values of expression fold-inductions after treatment are relative to the corresponding expression values of non-treated plants for each time point, with the value for time zero assumed to be one. Data is the result of three biological replicates, each with three technical replicates (mean values ± SD; n = 3). The significance levels between relative mRNA levels at each time point and time 0 are reported only when $P \leq 0.05$. *, **, ***, **** *P* values ≤ 0.05, 0.01, 0.001 and 0.0001 respectively.

Fig. 8 Analysis of *AtCuAOα2* and *AtCuAOα3* tissue specific expression pattern upon IAA and MeJA treatments. **a**-**j** Light microscopy analysis by GUS staining of 7-day-old *AtCuAOα2*::*GFP-GUS* transgenic seedlings untreated (a, c, e, g, i) or treated with 10 µM IAA for 3 h (b, d) or with 50 µM MeJA for 24 h, (f, h, j). The staining reaction proceeded for 2 h. **a** and **b** Cotyledon apical zone showing a slight increase of GUS staining at the apical hydathode (b). **c** and **d** Shoot apex with newly formed expanding leaves showing an increase of promoter activity in the apical hydathode (d). **e** and **f** Cotyledon apical zone showing a strong increase of GUS staining at apical hydathode (f). **g** and **h** Cotyledon lateral zone showing increase of GUS staining at the external border (h). **i** and **j** Shoot apex with newly formed expanding leaves showing an increased promoter activity in the apical hydathode and leaflet margins (j). **k**-**r** Light microscopy analysis by GUS staining of 7-day-old *AtCuAOα3-promoter::GFP-GUS* transgenic seedlings untreated (k, m, o, q) or treated with 10 µM IAA for 3 h (l, n) or with 50 µM MeJA for 6 h (p, r). The staining reaction proceeded 2 h and 1 h for IAA and MeJA treatments, respectively. **k** and **l** Shoot apex showing an increase of GUS staining, particularly in stipules (l). **m** and **n** Mature root showing a clear increase of promoter activity in the vascular tissues (n). **o** and **p** Shoot apex showing an increase of GUS staining in stipules (p). **q** and **r** Hypocotyl/root junction showing a clear increase of promoter activity in the hypocotyl, and the mature root zone (r). **s** and **t** LSCM analysis of GFP signal and PI staining of 5-day-old *AtCuAOα3*::*GFP-GUS* transgenic seedlings untreated (s) or treated (t) with 50 µM MeJA for 2 h showing a stronger signal in the vascular tissue of treated plants. a-d, k-n bar = 200 µm; e-j, o-t, bar = 100 µm.

Fig. 9 Time-course analysis of *AtCuAOα2* and *AtCuAOα3* gene expression by RT-qPCR upon abiotic stress treatments (dehydration and recovery and leaf wounding). Gene expression was analyzed in 7-day-old WT seedlings untreated or treated for 0h (T0), 30 min dehydration (T1) (see inset graph) followed by 1 (T2), 3 (T3), 6 (T4) and 24 h (T5) recovery, or 0 (T0), 1, 3, 6 and 24 h after leaf wounding. The reported values of expression fold-inductions after treatment are relative to the corresponding expression values of non-treated plants for each time point, with the value

for time zero assumed to be one. Data is the result of three biological replicates, each with three technical replicates (mean values ± SD; n = 3). The significance levels between relative mRNA levels at each time point and time 0 are reported only when P ≤ 0.05. *, **, ***, **** *P* values ≤ 0.05, 0.01, 0.001 and 0.0001 respectively.

Fig. 10 Analysis of *AtCuAOα2* and *AtCuAOα3* tissue-specific expression pattern upon abiotic stress (leaf wounding and dehydration recovery) treatments. **a-f** Light microscopy analysis by GUS staining of 7-day-old *AtCuAOα2*::*GFP-GUS* transgenic seedlings untreated (a, b) or subjected to dehydration 30 min plus 3 h recovery (c, d), or to cotyledonary leaf wounding for 3 h (e, f). The staining reaction proceeded for 2 h in both treatments. **a, c, and e** Young leaves of untreated (a), subjected to dehydration recovery (c) or to cotyledonary leaf wounding (e). **b, d, and f** Cotyledon of untreated (b) subjected to dehydration recovery (d) or to wounding (f). **g-l** Light microscopy analysis by GUS staining of 7-day-old *AtCuAOα3-promoter::GFP-GUS* transgenic seedlings untreated (g, h) or treated with dehydration 30 min plus 3 h recovery (i, j), or with cotyledonary leaf wounding for 3 h (k, l). The staining reaction proceeded for 2 h in both treatments. **g, i** and **k** Petiole/apex junction of untreated (g), submitted to dehydration recovery (i) or to cotyledonary leaf wounding (k). **h, j and l** Root mature zone of untreated (h), submitted to dehydration recovery (j) or to cotyledonary leaf wounding (l). a-l, bar = 200 µm.

Fig. 11 Time-course analysis of *AtCuAOα2* and *AtCuAOα3* gene expression by RT-qPCR upon treatment with the polyamines putrescine e spermidine. Gene expression was analyzed in 7-day-old WT seedlings untreated or treated with 500 µM putrescine or 500 µM spermidine for 0 (T0), 1, 3, 6 and 24 h. The reported values of expression fold-inductions after treatment are relative to the corresponding expression values of non-treated plants for each time point, with the value for time zero assumed to be one. Data is the result of three biological replicates, each with three technical replicates (mean values ± SD; n = 3). The significance levels between relative mRNA levels at each time point and time 0 are reported only when P ≤ 0.05. *, **, ***, **** *P* values ≤ 0.05, 0.01, 0.001 and 0,0001 respectively.

Fig. 12 Analysis of *AtCuAOα2* and *AtCuAOα3* tissue specific expression pattern upon putrescine or spermidine treatment.**a-f** Light microscopy analysis by GUS staining of 7-day-old *AtCuAOα2*::*GFP-GUS* transgenic seedlings untreated (a, b) or treated with 500 µM Put (c, d), or with 500 µM Spd (e, f), for 3 h. The staining reaction proceeded for 2 h. **a, c, e** Shoot apex with newly formed expanding leaves showing an increase of promoter activity in the apical hydathode and leaf margins with Put (c) and Spd (e) treatment. Cotyledonary leaf apical zone showing an increase of GUS staining at the apical hydathode with Put (d) and Spd (f) treatment. **g-j** Light microscopy analysis by GUS staining of 7-day-old *AtCuAOα3-promoter::GFP-GUS* transgenic seedlings untreated (g, i) or treated with 500 µM Put for 1 h (h, j). The staining reaction proceeded for 2 h. **g** and **h** Root mature zone showing an increase of GUS staining in the vascular tissue after Put treatment (h). **i** and **j** Stipules showing an increased promoter activity after Put treatment (j). a-f, i, j, bar = 200 µm; g, h bar = 100 µm.

Fig. 13 Time-course analysis of *AtCuAOγ1* and *AtCuAOγ2* gene expression by RT-qPCR upon treatment with IAA (a, b), MeJA (c, d), ABA (e, f) and SA (g, h). Gene expression was analyzed in 7-day-old WT seedlings untreated or treated with 10 µM IAA, 50 µM MeJA, 100 µM ABA or 2mM SA for 0 (T0), 1, 3, 6 and 24 h. The reported values of

expression fold-inductions after treatment are relative to the corresponding expression values of non-treated plants for each time point, with the value for time zero assumed to be one. Data is the result of three biological replicates, each with three technical replicates (mean values ± SD; n =3). The significance levels between relative mRNA levels at each time point and time 0 are reported only when $P \leq 0.05$. *, **, ***, **** *P* values ≤ 0.05, 0.01, 0.001 and 0,0001 respectively.

Fig. 14 Analysis of *AtCuAOγ1* and *AtCuAOγ2* tissue specific expression pattern upon IAA, ABA and SA treatments. **a** and **b** Light microscopy analysis by GUS staining of 7-day-old *AtCuAOγ1*::*GFP-GUS* transgenic seedlings untreated (a) or treated (b) with 10 µM IAA for 3 h, showing an increase of GUS staining in the root transition/elongation zone (b). The staining reaction was allowed to proceed for 30 min. **c** and **d** Light microscopy analysis by GUS staining of 5-day-old *AtCuAOγ1*::*GFP-GUS* transgenic seedlings untreated (c) or treated (d) with 100 µM ABA for 24 h showing an increase of GUS staining in the root transition/elongation zone (d). The staining reaction proceeded for 2 h. **e** and **f** Light microscopy analysis by GUS staining of 7-day-old *AtCuAOγ1*::*GFP-GUS* transgenic seedlings untreated (e) or treated (f) with 2 mM SA for 3 h, showing a slight increase of GUS staining towards the ground tissues of the maturation root zone (f). The staining reaction proceeded for 5 min. **g-j** Light microscopy analysis by GUS staining of 7-day-old *AtCuAOγ2*::*GFP-GUS* transgenic seedlings untreated (g, i) or treated (h, j) with 10 µM IAA for 3 h, showing an increase of GUS staining in the root cap (columella) (h) and the stipules associated with the first emerging leaves (j). The staining reaction proceeded for 2 h. a-j, bar = 100 µm.

Fig. 15 Time-course analysis *AtCuAOγ1* and *AtCuAOγ2* gene expression by RT-qPCR upon abiotic stress treatments (dehydration and recovery and leaf wounding). Gene expression was analyzed in 7-day-old WT seedlings untreated or treated for 0h (T0), 30 min dehydration (T1) (see inset graph) followed by 1 (T2), 3 (T3), 6 (T4) and 24 h (T5) recovery, or 0 (T0), 1, 3, 6 and 24 h after leaf wounding. The reported values of expression fold-inductions after treatment are relative to the corresponding expression values of non-treated plants for each time point, with the value for time zero assumed to be one. Data is the result of three biological replicates, each with three technical replicates (mean values ± SD; n = 3). The significance levels between relative mRNA levels at each time point and time 0 are reported only when $P \leq 0.05$. *, **, ***, **** *P* values ≤ 0.05, 0.01, 0.001 and 0,0001 respectively.

Fig. 16 Analysis of *AtCuAOγ1* and *AtCuAOγ2* tissue specific expression pattern upon abiotic stress (cotyledonary leaf wounding and dehydration recovery) treatments. **a-f** Light microscopy analysis by GUS staining of 7-day-old *AtCuAOγ1*::*GFP-GUS* transgenic seedlings untreated (a, d), subjected to dehydration 30 min plus 3 h recovery (b) or 6 h recovery (e), or to cotyledonary leaf wounding for 3 h (c, f). The staining reaction proceeded for 2 h in both treatments. **a, b, and c** Petiole/apex junction of untreated seedlings (a), subjected to dehydration recovery (b) or to cotyledonary leaf wounding (c). **d, e, and f** Root apex of untreated (d) subjected to dehydration recovery (e) or to cotyledonary leaf wounding (f). **g-l** Light microscopy analysis by GUS staining of 7-day-old *AtCuAOγ2-promoter::GFP-GUS* transgenic seedlings untreated (g-i) or subjected to cotyledon wounding for 3 h (j-l). The staining reaction proceeded for 2 h. **g, h** and **i** Cotyledon (g), Petiole/apex junction (h) and root apex (i) of untreated seedlings. **j, k and l** Cotyledon (h), Petiole/apex junction (k) and root apex (l) subjected to cotyledon wounding. a-l, bar = 100 µm.

Fig. 17 Time-course analysis of *AtCuAOγ1* and *AtCuAOγ2* gene expression by RT-qPCR upon treatment with the polyamines putrescine e spermidine. Gene expression was analyzed in 7-day-old WT seedlings untreated or treated with 500 µM putrescine or 500 µM spermidine for 0 (T0), 1, 3, 6 and 24 h. The reported values of expression fold-inductions after treatment are relative to the corresponding expression values of non-treated plants for each time point, with the value for time zero assumed to be one. Data is the result of three biological replicates, each with three technical replicates (mean values ± SD; n = 3). The significance levels between relative mRNA levels at each time point and time 0 are reported only when $P \leq 0.05$. *, **, ***, **** *P* values ≤ 0.05, 0.01, 0.001 and 0,0001 respectively.

Fig. 18 Analysis of *AtCuAOγ1* and *AtCuAOγ2* tissue specific expression pattern upon putrescine treatment. **a-d** Light microscopy analysis by GUS staining of 7-day-old *AtCuAOγ1*::*GFP-GUS* transgenic seedlings untreated (a, c) or treated (b, d) with 500 µM putrescine for 1 h showing GUS staining in the apex/petiole junction and apical hydathodes (arrows) (b) and the root transition/elongation zone (d). The staining reaction was allowed to proceed for 2 h. **e-h** Light microscopy analysis by GUS staining of 7-day-old *AtCuAOγ2*::*GFP-GUS* transgenic seedlings untreated (e, g) or treated (f, h) with 500 µM putrescine for 3 h, showing GUS staining in the cotyledon apical hydathode (f) and in the root cap (columella) (h). The staining reaction proceeded for 2 h. a-h, bar = 100 µm.

a

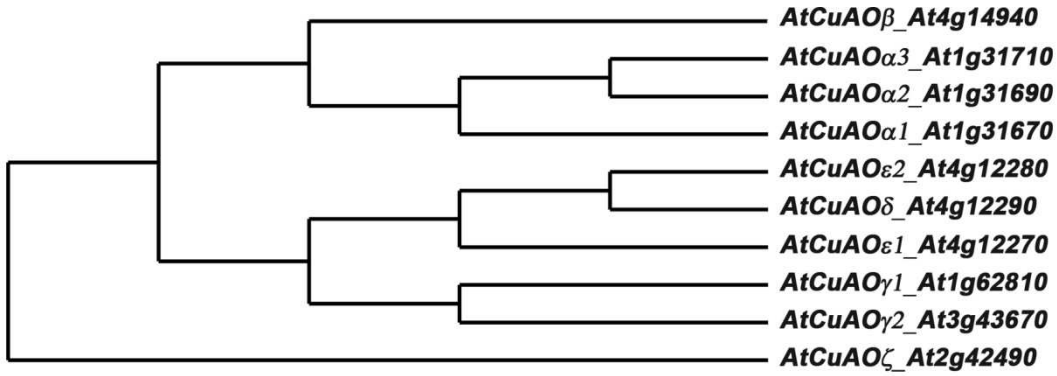

b

AtCuAOζ	100.00	28.21	30.86	25.55	27.25	27.92	28.03	27.22	27.88	28.01
AtCuAOγ1	28.21	100.00	77.00	48.22	58.59	67.24	44.67	44.80	45.47	45.76
AtCuAOγ2	30.86	77.00	100.00	49.13	57.37	67.60	41.97	43.55	43.38	43.82
AtCuAOε1	25.55	48.22	49.13	100.00	76.18	20.00	37.95	38.02	37.23	40.11
AtCuAOδ	27.25	58.59	57.37	76.18	100.00	91.30	43.95	44.18	44.11	47.04
AtCuAOε2	27.92	67.24	67.60	20.00	91.30	100.00	49.26	52.75	49.14	54.14
AtCuAOβ	28.03	44.67	41.97	37.95	43.95	49.26	100.00	49.52	47.83	50.23
AtCuAOα1	27.22	44.80	43.55	38.02	44.18	52.75	49.52	100.00	77.91	81.67
AtCuAOα3	27.88	45.47	43.38	37.23	44.11	49.14	47.83	77.91	100.00	80.21
AtCuAOα2	28.01	45.76	43.82	40.11	47.04	54.14	50.23	81.67	80.21	100.00

Additional file 1: Fig. S1 Phylogenetic analysis of AtCuAOs. Predicted amino acid sequences were retrieved by the online database "*The Arabidopsis Information Resource*" (TAIR) (https://www.arabidopsis.org). **A**, phylogenetic tree constructed by the online web service *Phylogeny.fr* (http://www.phylogeny.fr/simple_phylogeny.cgi) **B**, identity matrix made by the online web service *EMBL-EBI Clustal Omega* (http://www.ebi.ac.uk/Tools/msa/clustalo).

Additional file 2: Fig. S2 Alignment of AtCuAO and PSAO amino acids sequences. Alignment was performed by using the online web service *EMBL-EBI Clustal Omega* (http://www.ebi.ac.uk/Tools/msa/clustalo). The five active site residues essential for catalysis (Asp300, Tyr387, His442, His444 and His603; PSAO numbering) are highlighted in blue.

- *AtCuAOα2/α3 and AtCuAOγ1/γ2* present characteristic developmental-regulated profiles.
- *AtCuAOα2/α3* genes are induced by MeJA,
- *AtCuAOγ1* gene is induced by ABA and SA.
- IAA, Putrescine, Dehydration-recovery and wounding induce *AtCuAOs* expression.
- These *AtCuAOs* were expressed in vascular tissues, hydathodes and auxin-maximum zones.

Declaration of interests

☒ The authors declare that they have no known competing financial interests or personal relationships that could have appeared to influence the work reported in this paper.

☐The authors declare the following financial interests/personal relationships which may be considered as potential competing interests: